Copper and iron complexes containing the $M_2(\mu\text{-}O)_2$ core: syntheses, structures, and reactivities

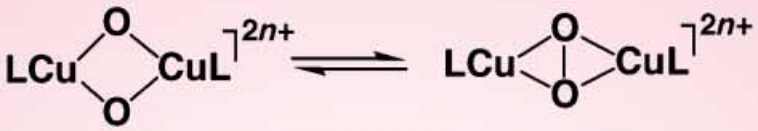

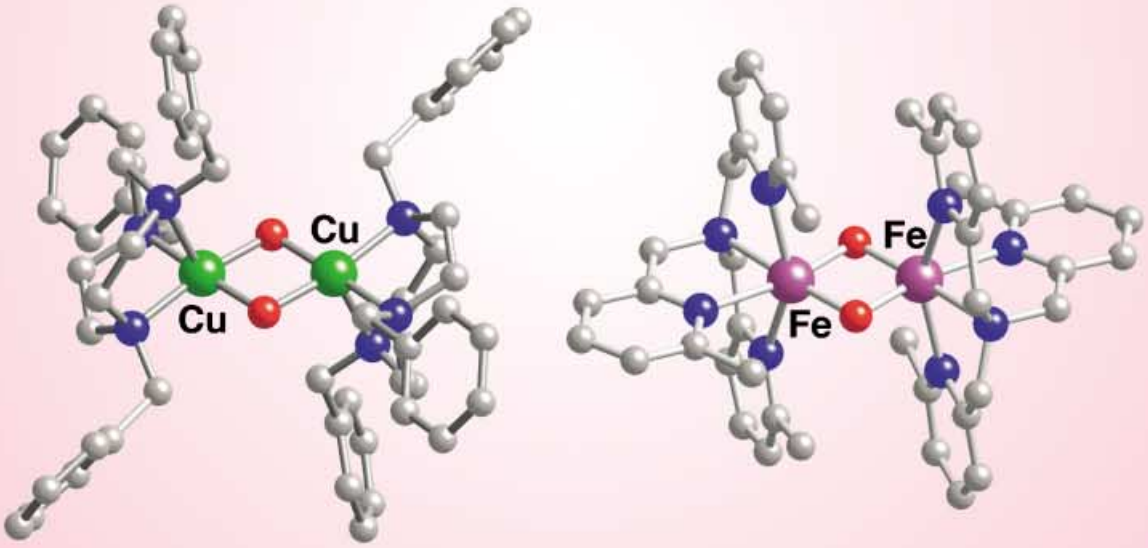

ANGEWANDTE
CHEMIE

Bis(μ-oxo)dimetal "Diamond" Cores in Copper and Iron Complexes Relevant to Biocatalysis

Lawrence Que, Jr.* and William B. Tolman*

Although quite a familiar feature in high-valent manganese chemistry, the $M_2(\mu\text{-}O)_2$ diamond core motif has only recently been found in synthetic complexes for M = Cu or Fe. Structural and spectroscopic characterization of these more reactive $Cu_2(\mu\text{-}O)_2$ and $Fe_2(\mu\text{-}O)_2$ compounds has been possible through use of appropriately designed supporting ligands, low-temperature handling methods, and techniques such as electrospray ionization mass spectrometry and X-ray crystallography with area detector instrumentation for rapid data collection. Despite differences in electronic structures that have been revealed through experimental and theoretical studies, $Cu_2(\mu\text{-}O)_2$ and $Fe_2(\mu\text{-}O)_2$ cores exhibit analogously covalent metal–oxo bonding, remarkably congruent Raman and extended X-ray absorption fine structure (EXAFS) signatures, and similar tendencies to abstract hydrogen atoms from substrates. Core isomerization is another common reaction attribute, although different pathways are traversed; for Fe, bridge-to-terminal oxo migration has been discovered, while for Cu, reversible formation of an O–O bond to yield a peroxo isomer has been identified. Our understanding of biocatalysis has been enhanced significantly through the isolation and comprehensive characterization of the $Cu_2(\mu\text{-}O)_2$ and $Fe_2(\mu\text{-}O)_2$ complexes. In particular, it has led to the development of new mechanistic notions about how non-heme multimetal enzymes, such as methane monooxygenases, fatty acid desaturase, and tyrosinase, may function in the activation of dioxygen to catalyze a diverse array of organic transformations.

Keywords: bioinorganic catalysis · copper · iron · metalloenzymes · metal–oxo complexes · oxygen activation

1. Introduction

Metal-promoted oxidations of organic compounds are of fundamental importance in organic synthesis, industrial catalysis, and enzymatic reactions. Chemists have long sought to unravel the mechanisms of such oxidations, with the ultimate objectives of inventing new reagents and exerting control over reactivity and selectivity. A key issue concerns the nature of the oxidizing species that is directly responsible for effecting the reaction. In some cases the oxidant is not metal-based (e.g. an organic radical derived from an autoxidation process), while in others a metal–oxygen species of some sort is implicated as the reactive intermediate.[1] Thorough characterization of such metal–oxygen species is critical for obtaining detailed mechanistic insights, but by their very nature as reactive oxidizing molecules they are difficult to isolate or even observe directly. The problem is exacerbated for oxidants comprising metal ions from the mid-to-late first-row transition series, such as iron and copper, that are particularly labile and active in many biochemically significant processes. These attributes are exemplified by heme–iron proteins and complexes, extensive studies of which have provided the mechanistic paradigm for dioxygen activation at a metal center.[2]

Recent work has centered on non-heme iron and copper sites in biology, in particular those with two proximal metal ions that yield novel oxidizing intermediates capable of performing diverse organic functionalizations.[3] Notable examples of these sites and corresponding structures for selected intermediates that have been postulated to be involved in their reactions are listed in Table 1.[3, 4] Significant insights into these dimetal systems have been attained through the synthetic modeling approach,[5] whereby the detailed characterization of O_2 adducts or derived species provides fundamental spectroscopic, structural, and reactivity benchmarks for understanding the metalloprotein sites and, ultimately, developing new catalysts.[6] Of particular consequence in this regard is the recent discovery of a new class of iron and copper complexes that contain the simple "diamond-

[*] Prof. Dr. L. Que, Jr., Prof. Dr. W. B. Tolman
Department of Chemistry and Center for Metals in Biocatalysis
University of Minnesota
207 Pleasant Street SE
Minneapolis, MN 55455 (USA)
Fax: (+1) 612-624-7029
E-mail: que@chem.umn.edu, tolman@chem.umn.edu

  1433-7851/02/4107-1115 $ 20.00+.50/0

Table 1. Examples of enzymes with non-heme diiron or copper active sites and key intermediates involved in catalysis.

Enzymes	Reaction catalyzed	Intermediates observed and *postulated* [a]	Ref.
methane monooxygenase	$CH_4 + O_2 + 2H^+ + 2e^- \rightarrow CH_3OH + H_2O$	MMOH-**P**: (μ-peroxo)diiron(III,III) MMOH-**Q**: bis(μ-oxo)diiron(IV,IV)	[3a,b,h]
fatty acid desaturase	$R(CH_2)_mCH_2{-}CH_2(CH_2)_nCOOH + O_2 + 2H^+ + 2e^- \rightarrow R(CH_2)_mCH{=}CH(CH_2)_nCOOH + 2H_2O$	(μ-1,2-peroxo)diiron(III,III), *bis(μ-oxo)diiron(IV,IV)*	[4a]
ribonucleotide reductase (cofactor generation)	$Fe^{II}Fe^{II} + Tyr122\text{-}OH + O_2 + H^+ + e^- \rightarrow Fe^{III}\text{-}O\text{-}Fe^{III} + Tyr122\text{-}O^{\bullet} + H_2O$	RNR-R2-**P**: (μ-1,2-peroxo)diiron(III,III) RNR R2-**X**: (μ-oxo)iron(III)iron(IV)	[3a,c, 4b]
ferritin (ferroxidase activity)	$4Fe^{II} + O_2 + 4H^+ \rightarrow 4Fe^{III} + 2H_2O$	(μ-1,2-peroxo)diiron(III,III)	[4c,d]
tyrosinase	$Tyrosine + O_2 + 2H^+ + 2e^- \rightarrow DOPA + H_2O \rightarrow dopaquinone + 2e^-$	(μ-η^2:η^2-peroxo)dicopper(II,II), *bis(μ-oxo)dicopper(III,III)*	[3d,f,i, 99]

[a] See Scheme 3 for illustrations.

shaped" $[M_2(\mu\text{-}O)_2]^{n+}$ core structure (Figure 1, M = Fe or Cu). While this bis(μ-oxo)dimetal motif is known for many complexes of metal ions from the early half of the first-row transition metal series (e.g. M = Ti,[7] V,[8] Cr,[9] Mn[10]) for which the complexes are usually quite stable, it had only been a figment of chemists' imaginations for complexes of the latter-half ions M = Fe, Co, Ni, or Cu until the recent successful synthetic work. New notions about how non-heme, multimetal enzymes function have arisen as a result of studies of these compounds.

In this Review we take a specific view towards uncovering general underlying chemical principles and drawing comparisons among the synthetic bis(μ-oxo)dimetal systems comprising iron and copper centers, with mention of species with

L. Que, Jr. W. B. Tolman

William B. Tolman (right) was born on May 20, 1961, in Cleveland, Ohio. As an undergraduate at Wesleyan University, Middletown, Connecticut (B.A. in 1983), he worked in the laboratory of Prof. Alan Cutler doing organometallic chemistry research. He obtained a Ph.D. in chemistry from the University of California, Berkeley, in 1987, under the advisorship of Prof. K. Peter C. Vollhardt. His interests shifted toward bioinorganic chemistry during a stint in the laboratory of Prof. Stephen J. Lippard at the Massachusetts Institute of Technology, where he was a National Institutes of Health and American Cancer Society Postdoctoral Fellow. He joined the faculty at the University of Minnesota in 1990 and currently is a Distinguished McKnight University Professor. He has received the Buck–Whitney Medal (American Chemical Society), a National Young Investigator Award (National Science Foundation), a Searle Scholar Award, a Camille and Henry Dreyfus Teacher-Scholar Award, and an Alfred P. Sloan Foundation Research Fellowship. Current research in his laboratory is focused on synthetic modeling of metalloprotein active sites and developing new catalysts for biodegradable polymer synthesis. Most of the rest of his time is spent happily with his wife, Bonnie, and three children, Sarah, Claire, and Simon.

Lawrence Que, Jr. (left) was born on April 23, 1949 in Manila, the Philippines, and obtained his Bachelor's degree in Chemistry from Ateneo de Manila University in 1969. He then pursued graduate studies in coordination chemistry at the University of Minnesota under Prof. Louis H. Pignolet (Ph.D. 1973). After postdoctoral stints in bioinorganic chemistry with Prof. Richard H. Holm at the Massachusetts Institute of Technology and Professor Eckard Münck at the University of Minnesota, he joined the Cornell University faculty in 1977. In 1983 he returned to the University of Minnesota, where he is now 3M/Alumni Distinguished Professor of Chemistry and Co-Director of the Center for Metals in Biocatalysis. In addition, he is currently serving as the Chief Editor for the Journal of Biological Inorganic Chemistry. *Among his awards are an Alfred P. Sloan Foundation Research Fellowship and Research Career Development and MERIT Awards from the National Institutes of Health. His research interests have focused principally on unraveling the mechanisms of dioxygen activation by non-heme iron enzymes using both biophysical and biomimetic approaches, which allows his group to explore the spectroscopic and mechanistic properties of metalloenzymes as well as the design and synthesis of structural and functional models of these enzymes. A key aspect of the work in the past few years is the development of strategies for trapping and characterisation of important reaction intermediates, such as those discussed in this review. The biomimetic studies have also led to a new research direction in asymmetric and 'green' oxidation catalysis. His interests outside of science include enjoying the outdoors and supporting the performing arts, together with wife Deb and daughters Emily and Erin.*

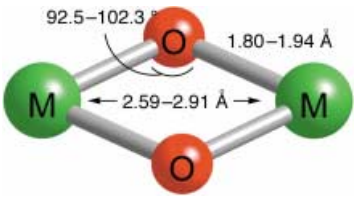

Figure 1. Range of selected interatomic distances and angles in bis(μ-oxo)-dimetal cores (see Table 3).

cobalt and nickel as well. These aims will be addressed through discussion of the extensive efforts to characterize the complexes by experimental and theoretical methods and to understand their reactivity. We then consider the relevance of these results to dioxygen activation processes in biological catalysis. Aspects of the chemistry presented here have been reviewed.[11–13]

2. Synthetic Considerations

2.1. General Comments

As mentioned above, complexes with the $[M_2(\mu\text{-}O)_2]^{n+}$ core have been known for many years for M = Mn with oxidation states (III,III), (III,IV), and (IV,IV).[10] These $[Mn_2(\mu\text{-}O)_2]^{n+}$ compounds are thermodynamically quite stable, and they typically are isolated as crystalline solids that endure for long periods under ambient conditions. The situation for the latter half of the first row transition metal ions M = Fe, Co,[14] Ni,[14–17] or Cu is rather different, insofar as these bis(μ-oxo)dimetal cores tend to be rather reactive and unstable at room temperature. The successful isolation and characterization of complexes of these metals was made possible by the use of two key synthetic strategies: a) low-temperature handling of solutions and solids to slow undesired decomposition reactions, and b) use of chelating supporting ligands, usually with alkyl substituents, that facilitate crystallization and inhibit intermolecular interactions (Scheme 1). These methods have precedents, in particular for the isolation of heme–iron and copper complexes with oxo, superoxo, or peroxo groups.[2, 6c, 18] Technological advances also have been critical for the recent successful characterization of the $[M_2(\mu\text{-}O)_2]^{n+}$ (M = Fe, Co, Ni, Cu) compounds; the availability of electrospray ionization mass spectrometry (ESI-MS)[19] and area detector X-ray diffraction instrumentation for rapid data collection on temperature-sensitive solutions and crystals, respectively, has been of particular value. Finally, the development of reproducible preparations of suitably designed precursor molecules is a key prerequisite in most synthetic endeavors, and extensive efforts toward this end were necessary to obtain the target bis(μ-oxo) complexes in sufficient purity and quantity for thorough characterization.

The methods used in attempts to prepare the bis(μ-oxo)diiron and -dicopper compounds have involved reactions of the generalized type shown in Equations (1)–(3) (not all balanced). In the reaction in Equation (1) four-electron reduction of O_2 is accomplished by a Cu^I precursor, which

$$2\,LCu^{I} + O_2 \rightarrow [(LCu^{III})_2(\mu\text{-}O)_2] \quad (1)$$

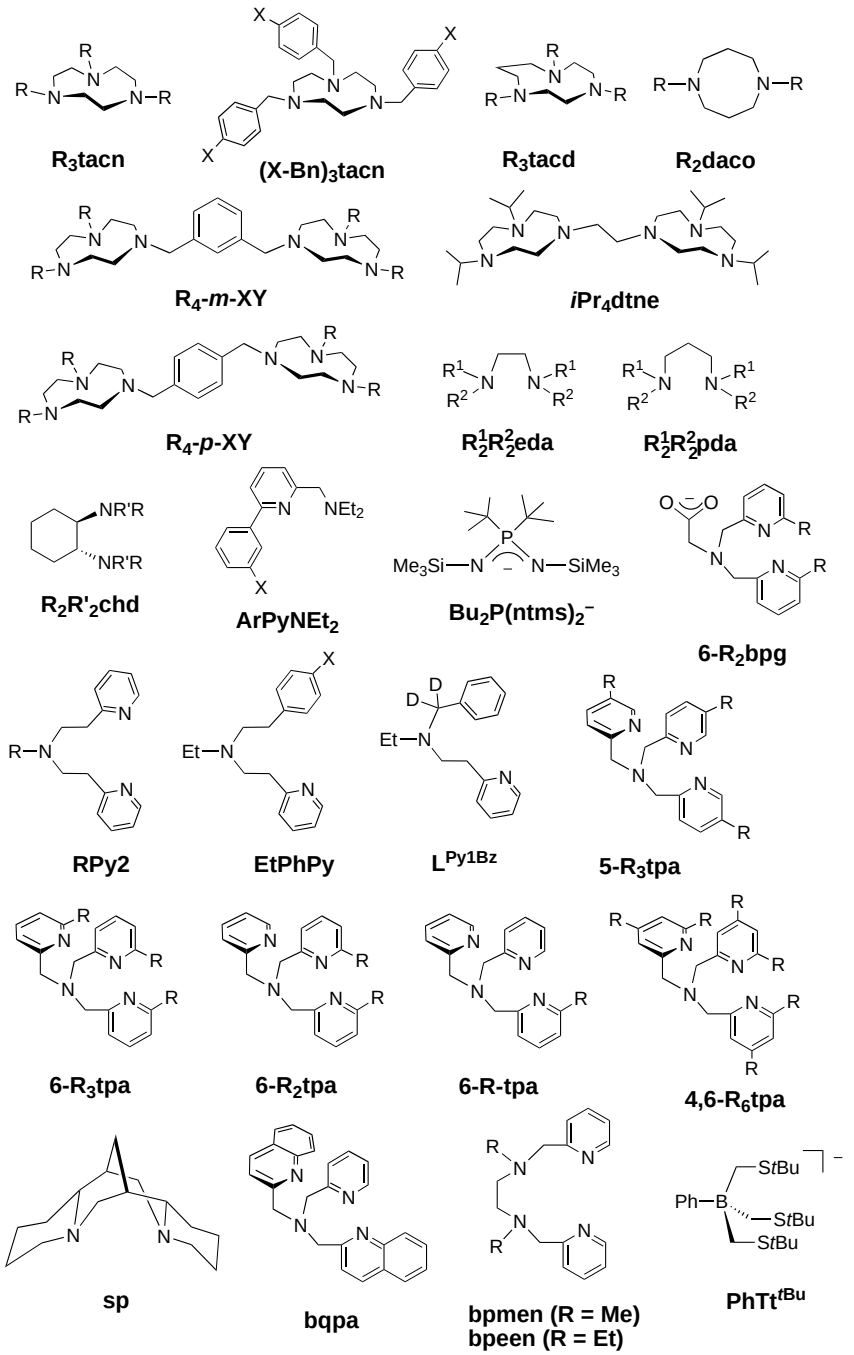

Scheme 1. Ligands used to prepare complexes with $[M_2(\mu\text{-}O)_2]^{n+}$ cores, with abbreviations that are used in the text.

results in incorporation of both O atoms into the bis-(μ-oxo)dicopper core. This method has been the major one used for the isolation of the copper compounds, although it has been examined in a few instances in attempts to prepare iron congeners and in one case for nickel.[17] The route in Equation (2) involves the reduction of H_2O_2 by a diiron(III)

$$[(LFe^{III})_2(\mu\text{-}O)] + H_2O_2 + 1\,e^- \rightarrow [(LFe^{III})(LFe^{IV})(\mu\text{-}O)_2] + H_2O \qquad (2)$$

precursor, and resembles the so-called "shunt" pathway used in heme iron enzymes and complexes for the generation of monoiron-oxo intermediates.[2] A similar method has been used to convert bis(μ-hydroxo)dinickel(II,II) and -dicobalt(II,II) complexes into their respective bis(μ-oxo)dimetal(III,III) relatives.[14–16] Equation (3) depicts another route involving deprotonation of a bridging hydroxide ligand in a diiron(III,III) precursor. Specific details of the preparations used for the Cu and Fe cases are summarized in the following section.

$$[(LFe^{III})_2(\mu\text{-}O)(\mu\text{-}OH)] + \text{base} \rightarrow [(LFe^{III})_2(\mu\text{-}O)_2] \qquad (3)$$

2.2. Specific Syntheses

2.2.1. *Bis(μ-oxo)dicopper(III,III)*

Treatment of LCu^I complexes with O_2 (1 atm) at low temperatures ($< -40\,^\circ C$) is the usual method for the synthesis of the bis(μ-oxo)dicopper compounds, which have been prepared using a wide range of ligands (Schemes 1 and 2).[20–37] Product identification was accomplished through

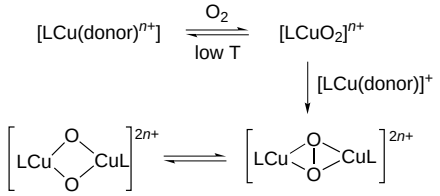

Scheme 2. Generalized course of the formation of bis(μ-oxo)dicopper complexes through the oxygenation of copper(I) precursors with supporting ligands L (Scheme 1). Donor = CH_3CN or $CH_2{=}CH_2$. Charges (n) are 1 for L = R_3tacn (R = Me, *i*Pr, aryl ether dendrimer), (X-Bn)$_3$tacn, ½*i*Pr$_4$dtne, ½*i*Pr$_4$-*p*-XY, R_2daco, $R_2R'_2$chd (R, R′ = Me, Et), $R^1_2R^2_2$pda, $R^1_2R^2_2$eda, MePy2, EtPhPy, 6-R_2tpa, and ArPyNEt$_2$; $n = 0$, L = $Bu_2P(ntms)_2^-$.

spectroscopic studies and, in selected instances, by X-ray crystallography and low-temperature ESI-MS. Mechanistic data for the oxygenation reaction are available in several instances from variable-temperature stopped-flow kinetics experiments.[21, 23, 24, 27] The data support the pathway shown in Scheme 2 involving initial formation of a 1:1 Cu:O_2 adduct, presumably a (superoxo)copper(II) species akin to previously identified examples (Scheme 3).[18, 38] This step is followed by trapping by a second Cu^I species to yield a (μ-peroxo)dicopper(II,II) intermediate that subsequently undergoes O–O bond breaking to afford the final bis(μ-oxo)dicopper(III,III) product. Product solutions and/or solids comprising only peroxo, only bis(μ-oxo), or mixtures of both have been identified, with the implication that the nature of the supporting ligand L is critical for determining whether or not the O–O bond breaks.

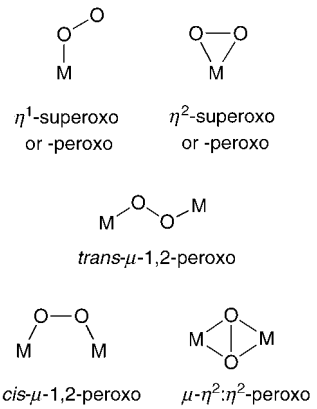

Scheme 3. Nomenclature for common metal–dioxygen adduct structures.

Direct evidence in support of the equilibrium in Scheme 2 between peroxo- and bis(μ-oxo)dicopper complexes is available in a few instances,[21, 33, 35, 39] but in others the evidence is indirect or not available. These issues are further discussed below in Section 6.1.

Although the overall pathway drawn in Scheme 2 appears to be general, differences in the relative rates of the individual steps have been observed. For the series of macrocyclic ligands L = R_2R'tacn (R = R′ = *i*Pr; R = *i*Pr, R′ = Bn; tacn = 1,4,7-triazacyclononane), *i*Pr$_4$-*m*-XY, and *i*Pr$_4$-*p*-XY, and ½*i*Pr$_4$dtne (dtne = 1,2-di(1,4,7-triaza-1-cyclononyl)ethane), the kinetic data show that 1:1 Cu:O_2 adduct formation is rate-determining, so that the rate of product (P) formation is described by the expression: $d[P]/dt = k[O_2][Cu^I\ \text{complex}]$. Selected activation parameters for this step are listed in Table 2. Mixtures of peroxo and bis(μ-oxo) species that must

Table 2. Selected activation parameters for oxygenations of Cu^I complexes.

Supporting ligand	$\Delta H^{\ddagger}$ [kJ mol^{-1}]	$\Delta S^{\ddagger}$ [J mol^{-1} K^{-1}]	Rate law[a]	Ref.
*i*Pr$_3$tacn	37.2(5)	−62(2)	$k[O_2][\text{complex}]$	[21]
*i*Pr$_4$-*m*-XY	39.4(5)	−30(2)	$k[O_2][\text{complex}]$	[24]
*i*Pr$_4$dtne	39.4(1)	−32.0(4)	$k[O_2][\text{complex}]$	[23]

[a] Rate law for the formation of bis(μ-oxo)- and/or peroxodicopper products.

rapidly equilibrate to explain the observed kinetics are seen for L = *i*Pr$_3$tacn, but sole bis(μ-oxo) complex generation occurs for L = Bn$_3$tacn, ½*i*Pr$_4$dtne, and *i*Pr$_4$-*p*-XY (as well as for other ligands for which oxygenation kinetics data are not available). For *i*Pr$_4$-*m*-XY the situation is more complicated because of competition between intramolecular peroxo and intermolecular bis(μ-oxo) complex formation after the initial O_2 binding step (Scheme 4).

Different kinetic behavior is observed for L = EtPhPy or RPy2 (R = $PhCH_2CH_2$; for structures see Scheme 1), where the rates of product formation have second-order dependencies on $[LCu^I]$.[27, 40] These findings suggest that the trapping of $LCuO_2$ by LCu^I is rate-controlling in these instances. Note that the observable product for the RPy2 case is the (μ-η^2:η^2-peroxo)dicopper complex and that a derived bis(μ-oxo)

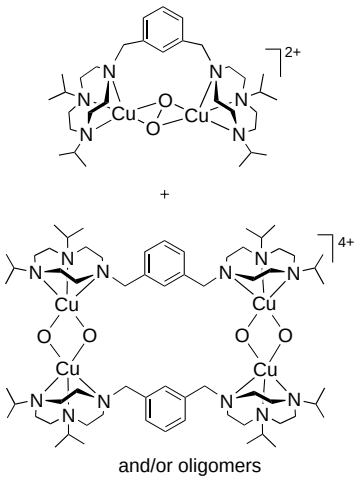

Scheme 4. The two products observed upon oxygenation of the dicopper(I,I) complex of iPr$_4$-m-XY, with the "intramolecular" adduct (top) favored in dilute solution (< 0.1 mM) and the "intermolecular" species (bottom) predominant at high concentrations (> 2.0 mM).[24]

species is only implicated from decomposition kinetics results. At this juncture, it is not clear what controls the relative rates of 1:1 adduct formation and subsequent trapping by Cu^I in the complexes that yield bis(μ-oxo) products, but these issues have been addressed for alternate copper-containing systems that form other types of oxygenated intermediates.[41]

2.2.2. *Bis(μ-oxo)diiron(III,III)*

The synthesis of the first crystallographically characterized bis(μ-oxo)diiron complex, a diiron(III,III) species,[42] was based on the facile acid/base/aquation chemistry outlined in Scheme 5.[43] The relative stabilities of the various species shown differ with the capping ligand L, and examples of each type have been structurally characterized. The complexes

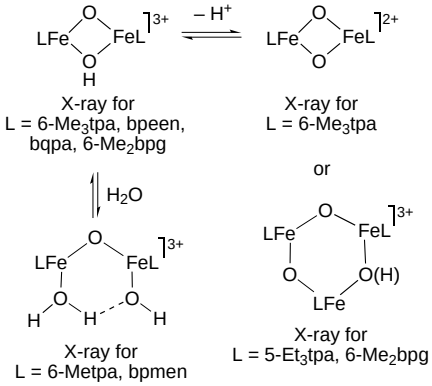

Scheme 5. Interconversions observed for various aqua, hydroxo, and oxo–iron species. Those that have been characterized by X-ray crystallography are so noted.[43, 47]

$[L_2Fe_2(\mu\text{-}O)(\mu\text{-}OH)]^{3+}$ are noteworthy because of the novelty of their core structure (previously seen only for M = Mn^{IV}[44] and Cr^{III}[45]) and their utility for drawing comparisons to bis(μ-oxo) species. They were prepared by oxidation of Fe^{II} salts by tBuOOH in the presence of L[43, 46] or by reaction of $[L_2Fe_2(\mu\text{-}O)(OAc)]^+$ with Et_3N in MeOH (L = 6-Me$_2$bpg; see Scheme 1).[47] These compounds serve as useful precursors of oxo-bridged polyiron(III) compounds by deprotonation reactions (pK_a values ≈ 16–18 in CH_3CN). In particular, for L = 6-Me$_3$tpa or 4,6-Me$_6$tpa, (for structures see Scheme 1) treatment of $[L_2Fe_2(\mu\text{-}O)(\mu\text{-}OH)]^{3+}$ (pK_a 15.9 and 16.3, respectively, in CH_3CN) with Et_3N yielded $[L_2Fe_2(\mu\text{-}O)_2]^{2+}$. With other ligands that lack the 6-Me substituents, trinuclear complexes form instead, $[L_3Fe_3(\mu_2\text{-}O)_3]^{3+}$ (L = 5-Et$_3$tpa) or $[L_3Fe_3(\mu_2\text{-}O)_2(\mu\text{-}OH)]^+$ (L = 6-Me$_2$bpg; Scheme 5).[43, 47]

2.2.3. *Bis(μ-oxo)diiron(III,IV) and Related Species*

Reaction of $[L_2Fe_2(\mu\text{-}O)(OH)(H_2O)]^{3+}$ (Scheme 6; L = tpa, 5-Me$_3$tpa, or 5-Et$_3$tpa) with H_2O_2 at $T = -40\,^\circ$C leads to the generation of a deep green species.[48] On the basis of extensive data from spectroscopic, ESI-MS,[48] and X-ray crystallographic (L = 5-Et$_3$tpa) studies,[49] this species was identified as $[L_2Fe_2(\mu\text{-}O)_2]^{3+}$. As described in greater detail below, it is best described as a valence-delocalized molecule comprising a magnetically coupled low-spin ($S = ½$) Fe^{III}/low-spin ($S = 1$) Fe^{IV} pair that yields an overall $S = ³/₂$ ground state.

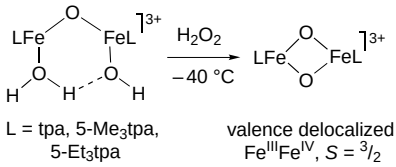

Scheme 6. Synthesis of $[L_2Fe_2(\mu\text{-}O)_2]^{3+}$, where L = tpa, 5-Me$_3$tpa, or 5-Et$_3$tpa.[48b, 49]

A related diiron(III,IV) complex with L = 6-Metpa was accessed in a similar way, but the relatively small difference in the ligand substituent pattern (6-H → 6-Me on one pendant pyridine) resulted in important electronic structural and, apparently, geometric changes (Scheme 7).[50] While the product formulation for L = 6-Metpa is $[L_2Fe_2(O)_2]^{3+}$, EPR

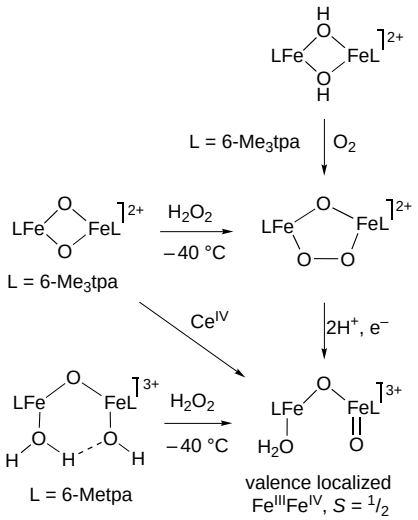

Scheme 7. Formation of diiron(III,IV) complexes supported by 6-Metpa or 6-Me$_3$tpa ligands.[50, 52, 53]

and Mössbauer spectroscopic results indicate that it contains a valence localized, antiferromagnetically coupled high-spin Fe^{III}/high-spin Fe^{IV} pair with an $S = ½$ ground state. Its spectral features resemble those of a key biological intermediate, compound "X" in ribonucleotide reductase (see Section 7).[3a,c] A species with similar properties results from treatment of $[L_2Fe_2(\mu\text{-}O)_2]^{2+}$ (L = 6-Me_3tpa) with H_2O_2.[51] In this instance, the high-valent species formed via an intermediate with a (μ-peroxo)(μ-oxo)diiron(III,III) core (Scheme 7). Oxygenation of a bis(μ-hydroxo)diiron(II,II) precursor capped by 6-Me_3tpa led to the same peroxo intermediate and high valent product.[52] In more recent work, this $S = ½$ product also was generated from chemical or electrochemical oxidation of $[L_2Fe_2(\mu\text{-}O)_2]^{2+}$ (L = 6-Me_3tpa) and the accumulated evidence indicated that it has one bridging and one terminal oxo unit derived from ring-opening isomerization of the bis(μ-oxo)diiron(III,IV) core.[53]

An $S = ½$ $Fe^{III}Fe^{IV}$ complex is also accessible with quite different supporting donors from those supplied by the tpa frame. Treatment of a CH_2Cl_2 solution of the paddlewheel complexes $[Fe_2(O_2CAr)_4(4\text{-}t\text{BuPy})_2]$ with O_2 at $-78\,^{\circ}C$ led to the formation of a metastable green solution which decomposed upon warming to yield a bis(μ-hydroxo)bis(μ-1,3-carboxylato)diiron(III,III) compound (Scheme 8).[54] On the basis of EPR and Mössbauer spectroscopic data, it was suggested that the green solution contained a mixture of three species: 1) an antiferromagnetically coupled diiron(III,III) complex, 2) an $S = 9/2$ $Fe^{II}Fe^{III}$ compound that is the green chromophore,[55] and 3) an $S = ½$ $Fe^{III}Fe^{IV}$ complex. The latter species was postulated to contain a bis(μ-oxo) motif on the basis of the literature evidence available at the time, but the recent identification of the isomeric bridging/terminal oxo arrangement for at least one of the $S = ½$ species (L = 6-Me_3tpa, derived from chemical oxidation)[53] suggests that this alternate structure should be considered.

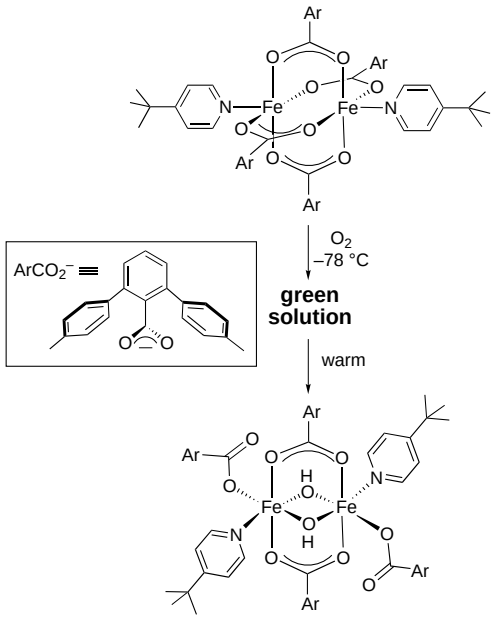

Scheme 8. Oxygenation of a diiron(II,II) complex supported by a sterically hindered carboxylate ligand.[54, 55]

3. X-ray Structures

Characterization of the bis(μ-oxo)dicopper and -diiron complexes by X-ray crystallography has been critical for conclusively identifying their novel cores, enabling detailed analysis of spectroscopic and physicochemical data, and providing a solid foundation for the drawing of comparisons to data acquired on relevant metalloproteins. The thermal instability of the complexes rendered such characterization difficult, but application of low-temperature handling techniques and rapid data-collection methods by using area detector instrumentation resulted in a number of successful structure determinations. Selected interatomic distances and angles for all complexes with $[M_2(\mu\text{-}O)_2]^{n+}$ (M = Cu or Fe) cores reported to date are listed in Table 3. For comparative purposes, data for selected compounds with Ni[14, 15, 17] and Co[14] cores and those with related core structures (e.g., hydroxo-bridged) also are listed.

A survey of the parameters shown in Table 3 reveals a general similarity among a wide variety of complexes with the bis(μ-oxo)dimetal motif; this is summarized in the schematic representation in Figure 1. In spite of differences in the metal ions, their oxidation level, and the supporting ligands, a relatively narrow range of distances and angles is observed for the $[M_2(\mu\text{-}O)_2]^{n+}$ unit. This lack of variation in structural parameters with differences in metal oxidation state and ligands was previously noted for M = Mn,[10] but must now be extended to include disparate metal ions with differing coordination numbers as well. As shown in Figure 1, the important general characteristics of the core that in combination distinguish it from related structures are the short intermetal and metal-oxo distances, essentially planar M_2O_2 arrangement, and acute M-O-M angles. Replacement of a μ-oxo bridge(s) with a μ-hydroxo unit(s) usually results in core expansion as reflected in lengthened M···M and M–O distances and larger M-O-M angles, although the presence of additional bridging ligands such as carboxylates can counteract this effect.[56, 57] Specific comparisons are described in greater detail below.

3.1. Copper

Representations of the X-ray structures reported to date of bis(μ-oxo)dicopper complexes are shown in Figure 2. While they have analogous $[Cu_2(\mu\text{-}O)_2]^{2+}$ core metrical parameters (Table 3, entries 1–4 and 6), differences in metal coordination numbers and geometries correlate with the number of N-donors in the different supporting ligands. Thus, each copper ion is four-coordinate square planar with the bidentate Me_2Et_2chd[26] or $Bu_2P(ntms)_2^-$[32] (for structures see Scheme 1) ligands, five-coordinate square pyramidal with the facially coordinating tridentate Bn_3tacn and $i\text{Pr}_4dtne$,[21–23] ligands and six-coordinate distorted octahedral with the tetradentate tripodal 6-Me_2tpa ligand.[30] The neutral complex supported by the $Bu_2P(ntms)_2^-$[32] ligand is somewhat anomalous with respect to its core geometry, as it exhibits rather long Cu···Cu and Cu–O distances (Table 3, entry 6). As would be expected for copper in the +III or +II oxida-

Table 3. Structural data for bis(μ-oxo)dimetal and related complexes.[a]

Entry	Core	Supporting ligands[b]	M···M	M–O	∢M-O-M	Ref.
1	$Cu_2^{III}(\mu\text{-}O)_2$	Me_2Et_2chd	2.743(1)	1.814(6) 1.809(6) 1.796(6) 1.804(6)	98.9(3) 98.8(3)	[26]
2		Bn_3tacn[c]	2.794(2)	1.803(5) 1.808(5)	101.4(2)	[21, 22]
3		$i Pr_4dtne$[c]	2.793(1)	1.827(4) 1.836(4) 1.824(4) 1.823(4)	99.3(2) 99.0(2)	[23]
4		6-Me_2tpa	2.758(4)	1.806(9) 1.799(8)	99.8(4)	[30]
5		MePy2[d]	3.445(2)	1.905(5) 1.922(6)	128.4(3)	[28]
6		$Bu_2P(ntms)_2^-$	2.906(1)	1.865 (3) 1.864(3)	102.3(2)	[32]
7		Et_4eda[e]	2.75	1.80		[77a]
8		Me_4pda[e]	2.85	1.81		[34]
9	$Fe^{III}Fe^{IV}(\mu\text{-}O)_2$	5-Et_3tpa	2.683(1)	1.805(3) 1.860(3)	94.07(1)	[49]
10		5-Me_3tpa[e]	2.59	1.77 1.94		[48b]
11	$Fe_2^{III}(\mu\text{-}O)_2$	6-Me_3tpa	2.716(2)	1.844(3) 1.916(4)	92.5(2)	[42, 43]
12	$Fe_2^{III}(\mu\text{-}O)(\mu\text{-}OH)$	bpeen	2.835(1)	1.850(3) 1.976(4) 1.846(3) 1.993(4)	91.1(2) 100.2(2)	[42]
13		Me_2bpg	2.899(2)	1.873(8) 1.962(6)	91.5(3) 103.9(4)	[47]
14	$Fe_2^{III}(\mu\text{-}OH)_2$	4-Me_2Ndipic[f]	3.118(3)	1.937(6) 1.986(9)	105.3(4)	[61b]
15		$ArCO_2^-$, Bn_2en/Bnen[g]	2.9788(6)	1.9726(17) 1.9977(17) 1.9852(17) 1.9805(16)	96.97(7) 97.64(7)	[56]
16		$ArCO_2^-$, pyridine[h]	2.8843(9)	2.012(2) 1.986(2)	92.33(10)	[57]
17	$Ni_2^{III}(\mu\text{-}O)_2$	Tp^{Me2}[i]	2.882(3)	1.841(7) 1.870(8)	101.9(3)	[14]
18		6-Me_3tpa	2.924(1)	1.888(6) 1.854(7)	102.8(3)	[15]
19		PhTt^{tBu}[c]	2.83	1.82		[17]
20	$Co_2^{III}(\mu\text{-}O)_2$	Tp^{Me2}[i]	2.728(2)	1.783(4) 1.796(5)	99.3(2)	[14]
21	$Ga_2^{III}(\mu\text{-}O)_2$	L^{dipp}[j]	2.5989(3)	1.8536(9) 1.8485(9)	88.18(4)	[64]

[a] Except where indicated, data are from X-ray crystal structures, distances [Å], angles [°], and estimated standard deviations indicated in parentheses. [b] Except where indicated, ligand abbreviations correspond to structures shown in Scheme 1. [c] Ligands with perdeuterated substituents were used. [d] Structural data (e.g. O···O = 1.666(12) Å) indicates compositional disorder (solid solution) of bis(μ-oxo)- and μ-η^2:η^2-peroxodicopper isomers. [e] Data are from EXAFS results. [f] 4-dimethylamino-2,6-dicarboxylatopyridine. [g] $ArCO_2^-$ = 2,6-ditolylbenzoate, with $[Fe_2(\mu\text{-}OH)_2(1,2\text{-}\mu\text{-}ArCO_2)_2]^{2+}$ core. [h] $ArCO_2^-$ = 2,6-ditolylbenzoate, Bn_2en = *N*,*N*-dibenzylethylenediamine, Bnen = N-benzylethylenediamine, with $[Fe_2(\mu\text{-}OH)_2(1,2\text{-}\mu\text{-}ArCO_2)]^{3+}$ core. [i] Tp^{Me2} = tris(3,5-dimethylpyrazolyl)hydroborate. [j] L^{dipp} = 2,4-bis(2,6-diisopropylphenylimido)pentane.

tion levels, distances between the metal ion and the axial donors in the square-pyramidal and distorted octahedral-geometries are elongated relative to the equatorial metal–ligand separations (data not listed). The axial donors adopt an *anti* arrangement in the Bn_3tacn-supported case, but they are *syn* in the complex with $i Pr_4$dtne as a result of the constraints of the ethylene tether between the macrocycles in this ligand. The $i Pr_4$dtne tether also appears to induce a slight distortion of the bis(μ-oxo) core from planarity, as indicated by the dihedral angle between the O-Cu-O and Cu-O-Cu planes of $\sim 13^\circ$.[23]

It is useful to compare the structural features common to the $[Cu_2(\mu\text{-}O)_2]^{2+}$ cores to those of related $[Cu_2(\mu\text{-}OH)_2]^{2+}$ and $[Cu_2(\mu\text{-}\eta^2\text{:}\eta^2\text{-}O_2)]^{2+}$ units supported by similar ligands (Figure 3).[22, 58] As noted above, the intermetal and metal–oxygen distances are increased in the $[Cu_2(\mu\text{-}OH)_2]^{2+}$ core. However, caution should be exercised in differentiating bis(oxo)- from bis(hydroxo)dicopper cores on the basis of intermetal separations alone, since a long Cu···Cu separation of 2.906(1) Å was seen in the neutral bis(μ-oxo)dicopper complex supported by $Bu_2P(ntms)_2^-$ ions.[32] The Cu···Cu separation in the (μ-η^2:η^2-peroxo)dicopper isomer of the

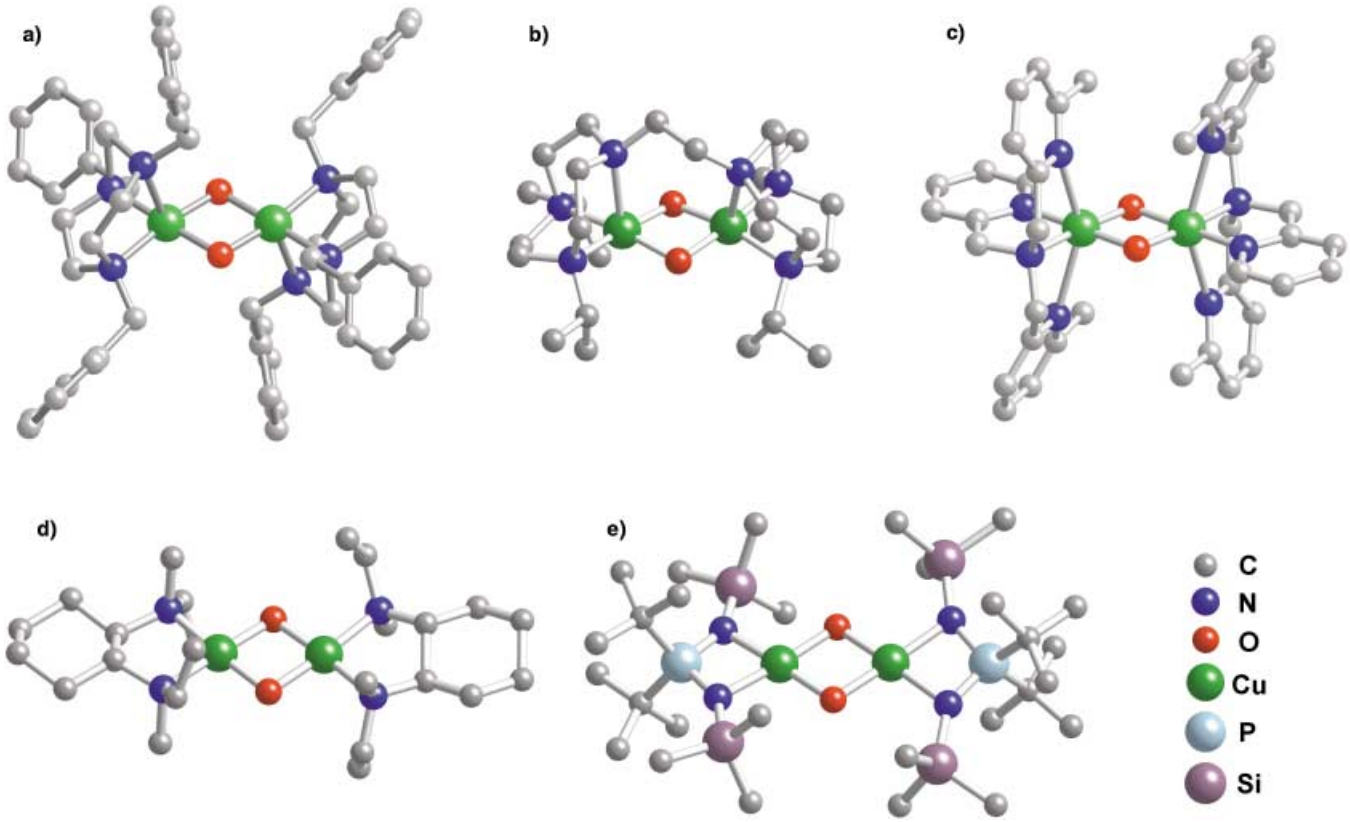

Figure 2. X-ray crystal structures of a) $[([D]_{21}\text{-}Bn_3tacn)_2Cu_2(\mu\text{-}O)_2]^{2+}$,[21, 22] b) $[([D]_{28}\text{-}i\text{Pr}_4dtne)Cu_2(\mu\text{-}O)_2]^{2+}$,[23] c) $[(6\text{-}Me_2tpa)_2Cu_2(\mu\text{-}O)_2]^{2+}$,[30] d) $[(Me_2Et_2chd)_2Cu_2(\mu\text{-}O)_2]^{2+}$,[26] and e) $[(Bu_2P(ntms)_2)_2Cu_2(\mu\text{-}O)_2]$.[32]

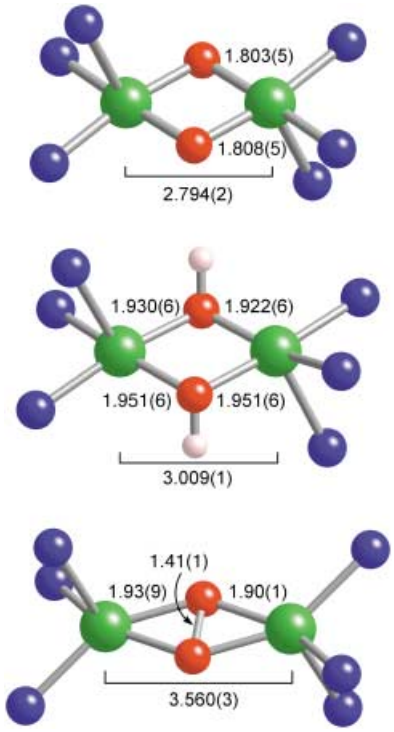

Figure 3. Comparison of prototypical $[Cu^{III}_2(\mu\text{-}O)_2]^{2+}$ (top), $[Cu^{II}_2(\mu\text{-}OH)_2]^{2+}$ (middle), and $[Cu^{II}_2(\mu\text{-}\eta^2\text{:}\eta^2\text{-}O_2)]^{2+}$ (bottom) cores from the respective X-ray structures of $[([D]_{21}\text{-}Bn_3tacn)_2Cu_2(\mu\text{-}O)_2](SbF_6)_2$,[21, 22] $[(i\text{Pr}_2\text{Htacn})_2Cu_2(\mu\text{-}OH)_2](BPh_4)_2$,[22] and $[Tp^{iPr2}_2Cu_2(\mu\text{-}\eta^2\text{:}\eta^2\text{-}O_2)]$.[58] Selected interatomic distances [Å] are indicated, with estimated standard deviations given in parentheses.

bis(μ-oxo) core is much larger[59] and this difference is accompanied by a decreased O–O distance indicative of a bond between these atoms.[58, 60] The metal–ligand bond distances in the $[Cu_2(\mu\text{-}OH)_2]^{2+}$ and $[Cu_2(\mu\text{-}\eta^2\text{:}\eta^2\text{-}O_2)]^{2+}$ cores are generally longer than in the bis(μ-oxo)dicopper compounds, a fact which is consistent with the Cu^{II}_2 assignment for the two former species and Cu^{III}_2 for the latter (see Section 5).

3.2. Iron

Figure 4 illustrates features of the cores found in several representative diiron complexes with bridging oxo and/or hydroxo ligands. Only one X-ray structure of a bis(μ-oxo)diiron(III,III) complex, $[(6\text{-}Me_3tpa)_2Fe_2(\mu\text{-}O)_2](ClO_4)_2$, is available.[42, 43] While its overall topology closely resembles those of the bis(μ-oxo)dicopper and -nickel complexes supported by the same 6-Me_3tpa or similar 6-Me_2tpa ligands (Figure 2),[15, 30] several unique aspects of the diiron core structure are worth noting (Table 3, entry 11). First, the Fe-μ-O bond lengths differ significantly, with one short bond *trans* to the ligand amine N atom (1.844(3) Å) and a longer bond *trans* to a pyridine donor atom (1.916(4) Å). This pronounced asymmetry in the core ($\Delta r = 0.076$ Å) is mirrored in $[Fe_2(\mu\text{-}OR)_2]^{4+}$ complexes (R = H or alkyl/aryl),[61] but contrasts with the more similar distances observed in bis(μ-oxo)dimetal compounds with M = Cu, Mn, V, or Cr. The Fe-μ-O distances are notably longer than in diiron(III,III) complexes with a

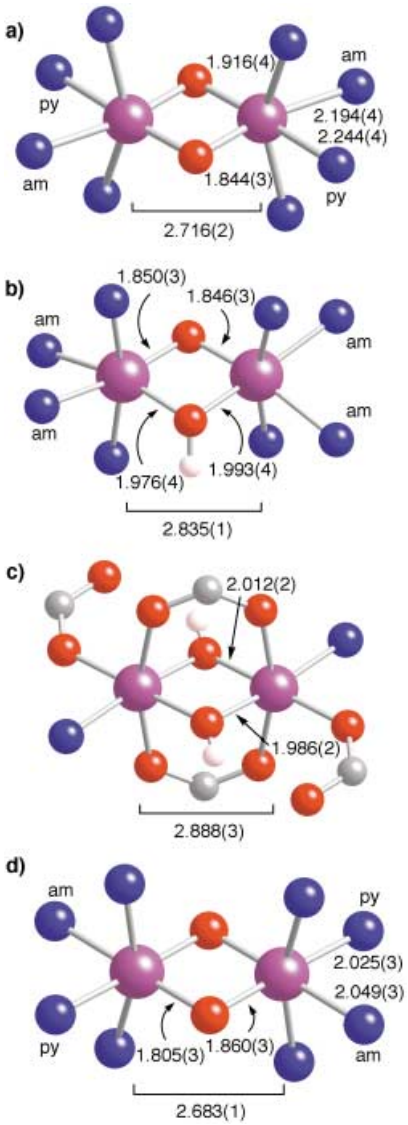

Figure 4. Comparison of the cores a) $[Fe^{III}_2(\mu\text{-}O)_2]^{2+}$, b) $[Fe^{III}_2(\mu\text{-}O)(\mu\text{-}OH)]^{3+}$, c) $[Fe^{III}_2(\mu\text{-}OH)_2(O_2CR)_2]^{2+}$, and d) $[Fe^{III}Fe^{IV}(\mu\text{-}O)_2]^{3+}$ from the respective X-ray structures of $[(6\text{-}Me_3tpa)_2Fe_2(\mu\text{-}O)_2](ClO_4)_2$,[42, 43] $[(bpeen)_2Fe_2(\mu\text{-}O)(\mu\text{-}OH)](ClO_4)_3$,[43] $[(py)_2(O_2CAr)_2Fe_2(\mu\text{-}OH)_2(\mu\text{-}O_2CAr)_2]$ (O_2CAr = 2,6-ditolylbenzoate),[57] and $[(5\text{-}Et_3tpa)_2Fe_2(\mu\text{-}O)_2](ClO_4)_3$.[49] Selected interatomic distances [Å] are indicated, with estimated standard deviations in parenthesis. The blue N atoms labeled "am" and "py" are amine and pyridyl donors, respectively.

single μ-oxo bridge (range 1.73 – 1.83 Å),[62] an observation that may be rationalized by invoking lessened Lewis acidity of the Fe^{III} ions as a result of the second μ-oxo bridge and greater steric interactions inherent in the compact $[Fe_2(\mu\text{-}O)_2]^{2+}$ core. This core is contracted compared to that of protonated forms[43, 61] (in the absence of additional bridges[54, 56, 57]), as reflected in the trend in Fe ··· Fe distances: $[Fe_2(\mu\text{-}O)_2]^{2+} < [Fe_2(\mu\text{-}OH)(\mu\text{-}O)]^{3+} < [Fe_2(\mu\text{-}OH)_2]^{4+}$ (Table 3, entries 11 – 14). A similar trend has been noted for a series of Mn^{III} complexes.[63] In addition, the Fe-μ-O-Fe angles are smaller than the Fe-μ-OH-Fe ones. Finally, it is noteworthy in the current context that a recently prepared bis(μ-oxo)digallium(III,III) complex supported by bidentate β-diketiminate ligands has a particularly short metal – metal distance and acute Ga-O-Ga angle (Table 3, entry 21).[64]

Consistent with its higher oxidation level and its spin state, metal – ligand bond distances in the low-spin diiron(III,IV) complex $[(5\text{-}Et_3tpa)_2Fe_2(\mu\text{-}O)_2](ClO_4)_3$ are shorter than in the high-spin bis(μ-oxo)diiron(III,III) compound (Table 3, entries 9 – 11).[49] Nonetheless, the Fe ··· Fe distances and Fe-O-Fe angles are similar in the two compounds, again attesting to the relative structural invariance of the bis(μ-oxo)dimetal unit. Another similarity is the asymmetry in the core Fe-μ-O distances [$\Delta r = 0.055$ Å for the diiron(III,IV) case], further corroborating the aforementioned generality of this feature in diiron(III and/or IV) systems.

4. Spectroscopic Signatures

In the absence of X-ray crystallographic information, the presence of an $M_2(\mu\text{-}O)_2$ core structure may be deduced by spectroscopic methods, of which the most directly diagnostic are extended X-ray absorption fine structure (EXAFS) and resonance Raman (rR) spectroscopies. The EXAFS region (above the edge jump) of an X-ray absorption spectrum of a metal complex contains information regarding the nature of the atoms surrounding the metal center and their distances from the metal center.[65] The r′-space EXAFS spectrum of a complex with an $M_2(\mu\text{-}O)_2$ core generally contains two prominent features,[17, 21, 22, 28, 34, 46, 48b, 49, 66] exemplified for M = Fe in Figure 5a, b. One is typically found at $r \approx 2$ Å and corresponds to the first coordination sphere (white arrow). This feature consists of the short (1.8 Å) M–O bonds that make up the core and the longer (2.0 – 2.1 Å) M-O/N bonds of the terminal ligands. Because of their > 0.2 Å difference, these two shells can usually be resolved in the EXAFS fitting protocol. The second feature is typically found at $r = 2.6$ – 2.9 Å (black arrow) and is associated with scattering between the two metal centers in the $M_2(\mu\text{-}O)_2$ core. Because of the presence of the two oxo bridges, the metal – metal distance is constrained to be less than 3 Å and the M-O-M angle approaches 90°. These properties distinguish the $M_2(\mu\text{-}O)_2$ core from other dinuclear motifs found in metalloproteins such as $M_2(\mu\text{-}\eta^2\text{:}\eta^2\text{-}O_2)$, $M_2(\mu\text{-}O)(O_2CR)_x$, and $M_2(O_2CR)_x$ cores, which usually have metal – metal distances greater than 3 Å and much larger M-O-M angles. Furthermore, independent movements of the two metal ions in the $M_2(\mu\text{-}O)_2$ unit are significantly limited. Thus, their motions are highly correlated, which leads to an intensity for the outer-sphere feature (black arrow) that is comparable to that arising from the first coordination-sphere atoms. This effect is operative even when the oxo bridges are protonated (Figure 5c and d). Note however that no outer-sphere feature is readily discerned for the paddlewheel complex $[Fe_2(O_2CtBu)_4(pyridine)_2]$ (Figure 5e), despite the fact that it has an Fe – Fe distance shorter than $[(6\text{-}Me_3tpa)_2Fe_2(\mu\text{-}O)(\mu\text{-}OH)]^{2+}$ (Figure 5c). The absence of the outer-sphere peak may be rationalized by the presence of a much less rigid core structure in $[Fe_2(O_2CtBu)_4(pyridine)_2]$, in which the metal ions are held together only by flexible, bidentate carboxylate bridges. Based on the examples shown, the presence of at least two single-atom

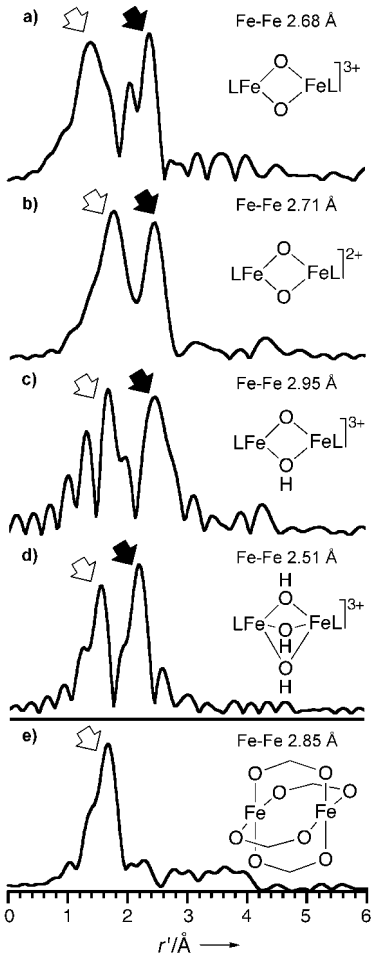

Figure 5. EXAFS spectra plotted in r' space ($r \approx r' + 0.4$) for a) $[Fe_2(\mu\text{-}O)_2(5\text{-}Me_3tpa)_2]^{3+}$, b) $[Fe_2(\mu\text{-}O)_2(6\text{-}Me_3tpa)_2]^{2+}$, c) $[Fe_2(\mu\text{-}O)(\mu\text{-}OH)(6\text{-}Me_3tpa)_2]^{3+}$, d) $[Fe_2(\mu\text{-}OH)_3(Me_3tacn)_2]^{2+}$, e) $[Fe_2(O_2CR)_4(pyridine)_2]$. First-shell features are indicated by the white arrow and the second-shell features (Fe – Fe scattering) are noted with a black arrow (a – d). Adapted with permission from ref. [49].

bridges are necessary to give rise to the strong intensity of the outer-sphere metal scattering. These principles also apply to complexes with M = Cu and Ni.[17, 20, 22, 28, 34] Thus, such an intense outer sphere feature is a convenient spectroscopic tool to determine the presence of an $M_2(\mu\text{-}O)_2$ core.

The $M_2(\mu\text{-}O)_2$ core also exhibits characteristic oxygen-isotope-sensitive features in vibrational spectra that are useful for identification purposes. Such vibrations are observed in Raman spectra upon excitation into an electronic absorption band having oxo → metal charge-transfer (CT) character (Section 5).[67–69] Simple symmetry considerations indicate that the $M_2(\mu\text{-}O)_2$ core has six core vibrations, three of which have the appropriate symmetry to be Raman active (Figure 6). In practice however, only the totally symmetric (A_g) modes are observed. Thus, for complexes with D_{2h} and C_{2h} (with the z axis in the M_2O_2 plane) symmetry, there are two vibrations with A_g symmetry; one involving significant M–O stretching called the "breathing" mode and the other a core bending mode. For complexes with C_{2h} symmetry where the z axis is perpendicular to the M_2O_2 plane, there is a third A_g mode designated the "pairwise" stretching mode.

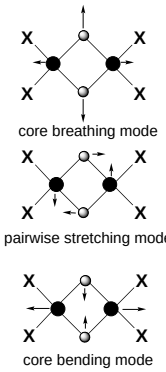

	estimated frequency [cm^{-1}]	D_{2h}	C_{2h} (C_2 in M_2O_2 plane)	C_{2h} ($C_2 \perp M_2O_2$ plane)
core breathing mode	≈ 600	A_g	A_g	A_g
pairwise stretching mode	≈ 600	B_{1g}	B_g	A_g
core bending mode	100–200	A_g	A_g	A_g

Figure 6. Frequencies and symmetry representations of important vibrational modes of bis(μ-oxo)dimetal cores in different point groups.

Complexes with $Fe_2(\mu\text{-}O)_2$ cores exhibit a prominent oxygen-isotope-sensitive Raman feature at 650 – 690 cm^{-1}.[67] Our understanding of this vibration derives from the large amount of structural and Raman information available for oxo-bridged diiron complexes.[62, 70] An Fe-O-Fe unit has two stretching vibrations that arise from the two Fe–O bonds. The extent to which the two vibrations are coupled depends on the M-O-M angle, with the strongest coupling found for linear Fe-O-Fe complexes. In these complexes, the symmetric combination $\tilde{\nu}_{sym}$(Fe-O-Fe) is observed in their Raman spectra at around 350 cm^{-1} and the asymmetric combination $\tilde{\nu}_{asym}$(Fe-O-Fe) is observed at approximately 850 cm^{-1} in their IR spectra, consistent with the respective symmetries of the vibrations and the selection rules associated with the two spectroscopic techniques. As the Fe-O-Fe angle becomes more acute, the coupling interaction weakens and the two vibrations start to converge to a common value.[70] Figure 7 displays the currently available vibrational data for structurally characterized oxo-bridged diiron complexes (open and closed circles) and demonstrates the correlation between the M-O-M angle and the $\tilde{\nu}_{sym}$(Fe-O-Fe) and $\tilde{\nu}_{asym}$(Fe-O-Fe) values. Note that at an M-O-M angle of 90°, where the two Fe–O bonds are orthogonal and the two Fe–O vibrations are independent of each other, the ν(Fe-O-Fe) values approach 650 cm^{-1}. The recent report of a ν(Fe–O) of 671 cm^{-1} for a mononuclear iron(III) – oxo complex supports this prediction.[71]

The symmetry of the Fe-O-Fe core plays an important role in determining the intensities of the Fe-O-Fe vibrations in the Raman spectrum. In complexes where the two iron coordination environments are essentially identical, only the allowed ν_{sym}(Fe-O-Fe) mode is observed as an intense peak. The forbidden ν_{asym}(Fe-O-Fe) mode would at best be observed as a very weak peak, so the intensity ratio I_{asym}/I_{sym} would be close to zero. As the asymmetry of the Fe-O-Fe unit increases, the ν_{asym}(Fe-O-Fe) mode becomes more easily observed in the Raman spectrum. For example, for the tpa complexes with a (μ-oxo)(μ-carboxylato)diiron(III,III) core such as the $[(tpa)_2Fe_2(\mu\text{-}O)(O_2CCH_3)]^{3+}$ ion the I_{asym}/I_{sym} ratio is around 0.2 because the oxo bridge is *trans* to the N atom of a pyridine group on one metal center and *trans* to an amine group N atom on the other.[72] A more dramatic example of an

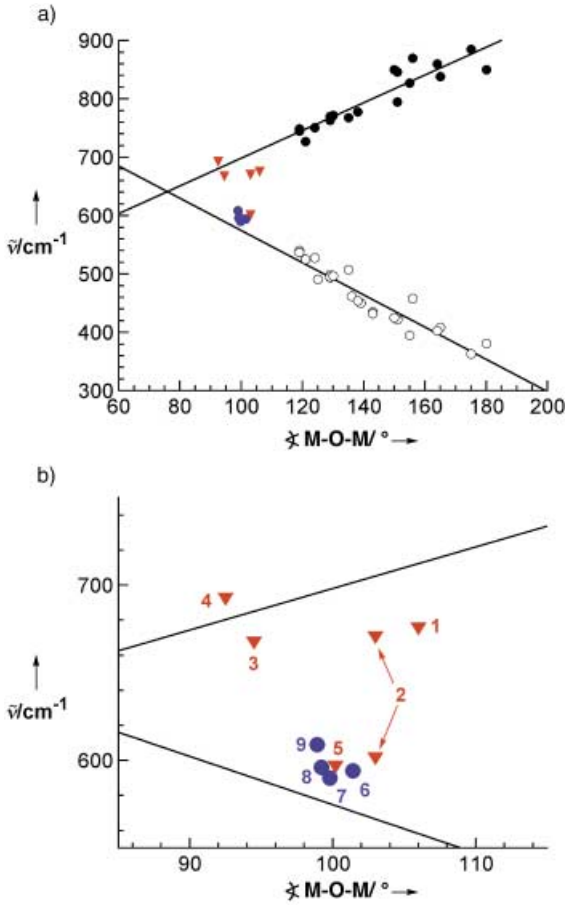

Figure 7. a) Plot of M-O-M angle versus $\tilde{\nu}_{sym}$ (○) and $\tilde{\nu}_{asym}$ (●) for a series of complexes containing Fe-O-Fe cores. Data for structurally characterized complexes with $Fe_2(\mu\text{-}O)_2$ and $Fe_2(\mu\text{-}O)(\mu\text{-}OH)$ cores are represented by ▼ and for $Cu_2(\mu\text{-}O)_2$ cores by ●. b) Expanded region of the plot in Figure 7a with labels refering to specific vibrations and complexes: **1**: ν_{asym} of $[(6\text{-}Me_3tpa)_2Fe_2(\mu\text{-}O)(\mu\text{-}OH)](ClO_4)_3$, **2**: ν_{asym} (top) and ν_{sym} (bottom) of $[(4,6\text{-}Me_6tpa)_2Fe_2(\mu\text{-}O)(\mu\text{-}OH)](ClO_4)_3$, **3**: ν_{asym} of $[(5\text{-}Me_3tpa)_2Fe_2(\mu\text{-}O)_2](ClO_4)_3$, **4**: ν_{asym} of $[(6\text{-}Me_3tpa)_2Fe_2(\mu\text{-}O)_2](ClO_4)_2$, **5**: ν_{sym} of $[(bpeen)_2Fe_2(\mu\text{-}O)(\mu\text{-}OH)](ClO_4)_3$, **6**: $[([D]_{21}\text{-}Bn_3tacn)_2Cu_2(\mu\text{-}O)_2](ClO_4)_2$, **7**: $[(6\text{-}Me_3tpa)_2Cu_2(\mu\text{-}O)_2](PF_6)_2$, **8**: $[([D]_{28}\text{-}i\text{Pr}_4dtne)Cu_2(\mu\text{-}O)_2](ClO_4)_2$, **9**: $[(Me_2Et_2chd)_2Cu_2(\mu\text{-}O)_2](CF_3SO_3)_2$. Adapted with permission from refs. [43, 67, 70], with additional data from ref. [67–69].

asymmetric Fe-O-Fe core is that of the $[(N5)Fe\text{-}O\text{-}FeCl_3]^+$ ion, [73] which features an octahedral metal center on one side and a tetrahedral metal center on the other. For this complex, the I_{asym}/I_{sym} ratio jumps to 4.2. The Fe^{II}-O-Fe^{III} unit of the mixed-valent $[(Me_3tacn)_2Fe_2(\mu\text{-}O)(O_2CR)_2]^+$ compound may be considered an extreme example of an asymmetric Fe-O-Fe core,[74] and only the ν_{asym}(Fe-O-Fe) mode is observed. Clearly, the Raman properties of the Fe-O-Fe core serve as sensitive probes of its symmetry properties.

The entries at low M-O-M angle in Figure 7 (red triangles, labeled specifically in Figure 7b) comprise compounds with diamond-shaped diiron cores; the introduction of a second single-atom bridge restricts the size of the M-O-M angle to 100° or less. For complexes with an $Fe_2(O)(OH)$ core, the M-O-M angle is about 100°. Interestingly the bpeen (for structure see Scheme 1) complex has its ν(Fe-O-Fe) feature at 596 cm^{-1}, while the 6-Me_3tpa complex has its feature at 675 cm^{-1}.[43] As indicated in Figure 7, the feature for the bpeen complex falls near the line for ν_{sym}(Fe-O-Fe), while that for the 6-Me_3tpa complex is closer to the line for ν_{asym}(Fe-O-Fe). The difference between the two complexes can be rationalized by considering their structures. The bpeen complex has a symmetric Fe-O-Fe unit with the oxo bridge *trans* to amine nitrogen atoms on both irons, so it displays an intense ν_{sym}(Fe-O-Fe) band. On the other hand, the oxo bridge is *trans* to an amine nitrogen atom on one iron and *trans* to a pyridine nitrogen atom on the other in the 6-Me_3-tpa complex, which results in greater intensity for ν_{asym}(Fe-O-Fe). Consistent with the fact that they have structures quite similar to that of $[(6\text{-}Me_3tpa)_2Fe_2(\mu\text{-}O)_2]^{2+}$, the high valent $[L_2Fe_2O_2]^{3+}$ complexes (L = tpa, 5-Me_3tpa, and 5-Et_3tpa) each exhibit just one major Raman peak with values that fall on the ν_{asym}(Fe-O-Fe) line. Thus, the correlation in Figure 7 applies not only to oxo-bridged diiron(III,III) complexes but also to oxo bridged $Fe^{II}Fe^{III}$ and $Fe^{III}Fe^{IV}$ complexes as well.

The fact that the Raman features of $Fe_2(\mu\text{-}O)_2$ complexes fit well into the correlation of ν(Fe-O-Fe) with M-O-M angle raises the question of whether the observed vibration is triatomic or is instead associated with a mode of the entire tetraatomic core. This question may be probed by introducing just one ^{18}O isotope into the Fe_2O_2 core. The assignment of the Raman feature to a triatomic vibration would be confirmed by the observation of two features in the spectrum of the mixed-labeled complex arising from ν(Fe-^{16}O-Fe) and ν(Fe-^{18}O-Fe) vibrations, with relative intensities reflecting the populations of the two isotopomers (e.g., equal intensities for a 1:1 ratio of ^{16}O:^{18}O). In contrast, a vibration that is tetraatomic in nature would exhibit a single feature with a value intermediate between the two $^{16}O^{16}O$- and $^{18}O^{18}O$-labeled extremes. For $[(tpa)_2Fe_2(\mu\text{-}O)_2]^{3+}$,[67] the $^{16}O^{16}O$ isotopomer exhibits a Raman peak at 666 cm^{-1} that shifts 28 cm^{-1} to lower energy in the $^{18}O^{18}O$ isotopomer. When ^{18}O is incorporated into only one oxygen atom of the $Fe_2(\mu\text{-}O)_2$ core, a single peak with an isotope shift of 22 cm^{-1} is observed. Thus, the iron–oxo vibration observed for $[(tpa)_2Fe_2(\mu\text{-}O)_2]^{3+}$ and related complexes derives from motion of the entire tetraatomic core.

Assignment of the 650–690 cm^{-1} band for the $Fe_2(\mu\text{-}O)_2$ complexes rests on their having C_{2h} symmetry with the C_2 axis perpendicular to the M_2O_2 core, such that there are two modes with totally symmetric A_g representations that are thus Raman allowed (Figure 6). One, designated the "breathing" mode, is analogous to the ν_{sym}(Fe-O-Fe) band of the triatomic Fe-O-Fe complexes. The other, designated the "pairwise" mode, is analogous to ν_{asym}(Fe-O-Fe). Normal coordinate analysis predicts both modes to be at similar frequencies, but the pairwise mode assignment is favored on the basis of several arguments.[67] There appears to be a weaker feature, observed at 655 cm^{-1} as a low-energy shoulder of the 666 cm^{-1} peak in the tpa complex, which is tentatively assigned as the breathing mode.

Similar considerations apply to the Raman spectra of complexes with $Cu_2(\mu\text{-}O)_2$ cores.[28, 68, 69] Those with symmetric bidentate ligands such as, $R_2R'_2$chd, $R^1_2R^2_2$eda, and $R^1_2R^2_2$pda have D_{2h} core symmetry and exhibit two core vibrations (Figure 6). The Raman data for the complex $[(Me_2Et_2\text{-}chd)_2Cu_2(\mu\text{-}O)_2]^{2+}$ is illustrative (Figure 8).[68] An intense

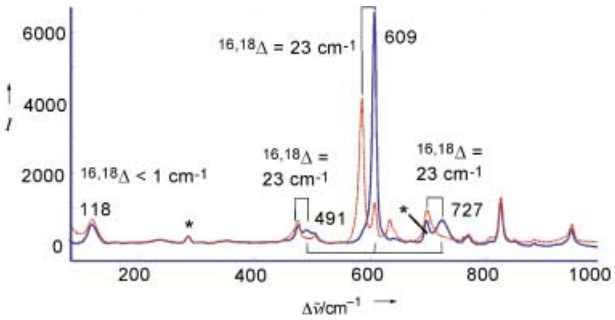

Figure 8. Resonance Raman spectra of $[(Me_2Et_2chd)_2Cu_2(\mu\text{-}O)_2](CF_3SO_3)_2$ in CH_2Cl_2, derived from $^{16}O_2$ (blue) and $^{18}O_2$ (red). Asterisks denote solvent peaks. Adapted with permission from ref. [68].

feature at 609 cm^{-1} corresponds to the core breathing mode; upon ^{18}O substitution it moves to lower energy by 24 cm^{-1}, in close agreement with the calculated value of 28 cm^{-1}. This intense feature is flanked by two much weaker features separated from the central peak by 118 cm^{-1} that move to lower energy by the same amount as the central feature when ^{18}O is incorporated. Examination of the low-frequency region reveals a feature at 118 cm^{-1}, which is assigned to the core bending mode. Thus, the features flanking the intense 609 cm^{-1} peak are combination and difference bands of the fundamental core breathing and core bending modes. Complexes of the other symmetric diamine ligands exhibit the same features at comparable energies. The fact that the two fundamental modes exhibit frequencies that are essentially independent of the nature of the ligand emphasizes the notion that these are indeed vibrations of the $Cu_2(\mu\text{-}O)_2$ core.

Replacement of the supporting diamines in the bis(μ-oxo)dicopper complexes with tridentate R_3tacn ligands lowers the point-group symmetry of the complexes to C_{2h}, as the copper ions adopt a square pyramidal geometry. Although the principal axis in these cases is coincident with the O–O axis, the symmetry designations for the core vibrations remain unchanged, so the same two totally symmetric Raman modes found for the D_{2h} complexes are expected for these C_{2h} complexes.[69] Indeed, all the R_3tacn complexes exhibit an intense ^{18}O isotope-sensitive vibration near 600 cm^{-1} that is assigned to the core breathing mode. However, no effort was made to observe the core bending mode in the low-frequency region. A notable difference between the data acquired for the R_3tacn and diamine complexes is an apparent sensitivity of the core breathing mode of the former to the mass of the supporting ligand alkyl substituents, with larger energy decreases as the mass of the alkyl substituent increases.

In $Cu_2(\mu\text{-}O)_2$ complexes with unsymmetric bidentate N-donor ligands the core symmetry also is C_{2h}, but the principal axis is perpendicular to the Cu_2O_2 core. For such complexes, both breathing and pairwise stretching modes belong to the totally symmetric A_g representation, which leads to the expectation of two observable features in the Raman spectrum. Indeed, two ^{18}O isotope-sensitive Raman features are observed in the 600 cm^{-1} region for the complexes $[(EtPhPy)_2Cu_2(\mu\text{-}O)_2]^{2+}$ and $[(ArPyNEt_2)_2Cu_2(\mu\text{-}O)_2]$.[25, 27] The appearance of two Cu–O stretching peaks is reminiscent of the two ν(Fe-O) features observed in the Raman spectra of Fe-O-Fe complexes with similarly unsymmetric ligands, as discussed above.[43] However, another complex which belongs to this class, $[(6\text{-}Me_2tpa)_2Cu_2(\mu\text{-}O)_2]^{2+}$, exhibits only one ^{18}O isotope-sensitive Raman feature in the 600 cm^{-1} region. The appearance of only one peak may be rationalized by the crystal structure of this complex, which shows a Cu_2O_2 core with four Cu–O bonds nearly equal in length, so the pairwise mode may not have much intensity. Unfortunately, X-ray crystal structures are not available for the two complexes that exhibit both core breathing and pairwise stretching modes.

When the core breathing modes observed for the Cu_2O_2 complexes are placed on the plot in Figure 7 (blue circles), they essentially fall on the ν_{sym}(M-O-M) line, which is consistent with the notion that the core breathing mode is the tetranuclear equivalent of the symmetric M-O-M stretching vibration. It may be surprising that the correlation derived from a database of iron compounds should also apply to copper complexes. Separate analysis of the latter is not possible because there is no database available for mono-oxo bridged dicopper complexes; few of these complexes exist,[18] none have been characterized structurally, and no Raman data have been reported. Nevertheless, there are a number of Fe^{III}-O-Cu^{II} complexes that have been synthesized to model the dioxygen binding and activation site of cytochrome *c* oxidase.[18a,b] One of these exhibits an Fe-O-Cu angle of 178° and a $\tilde{\nu}_{asym}$(Fe-O-Cu) at 855 cm^{-1},[75] in good agreement with the correlation in Figure 7. Thus, the differences in the atomic weights of Fe and Cu and in the relative strengths of the M–O bonds appear not to be large enough to affect the correlation in Figure 7 significantly.

In summary, EXAFS and resonance Raman spectroscopy represent two valuable tools that may be used to determine whether an $M_2(\mu\text{-}O)_2$ core is present in a sample. Indeed, these spectroscopic signatures were recognized in the EXAFS and Raman spectra of $[(R_3tacn)_2Cu_2(\mu\text{-}O)_2]^{2+}$ and $[(tpa)_2Fe_2(\mu\text{-}O)_2]^{3+}$ complexes prior to their characterization by X-ray crystallography.[20, 48] Similar approaches have been used to determine whether an $M_2(\mu\text{-}O)_2$ core is present in the reactions of other dicopper and diiron complexes with O_2 or H_2O_2.[28]

5. Electronic Structures

Not surprisingly, despite their similar geometric and vibrational properties the bis(μ-oxo)dimetal cores comprising iron and copper have differing electron inventories that result in divergent electronic structures. These structures have been probed by both experimental and theoretical methods. The $Cu_2(\mu\text{-}O)_2$ complexes are best characterized as having Cu^{III} ions bridged by two oxide ions. The Cu^{III} oxidation state description is supported by a bond valence sum (BVS) analysis of the crystallographic data[22, 76] and an analysis of X-ray absorption pre-edge energies.[77] In the BVS analysis, values for the copper-ion oxidation level consistently much larger than +2 were obtained when the structural data were analyzed using parameters derived from Cu^{II} complexes, while values close to +3 were obtained using parameters

associated with known Cu^{III} complexes. More direct information was gleaned from the X-ray absorption edges. Through an analysis of a large series of complexes, a clear distinction between those that contain Cu^{II} and those with Cu^{III} was drawn. While Cu^{II} complexes exhibit a $1s \rightarrow 3d$ pre-edge peak at 8979 ± 0.5 eV that is quite insensitive to changes in the ligand environment, the corresponding feature for Cu^{III} complexes is observed at 8981 ± 0.5 eV, consistently 2 eV higher in energy than its Cu^{II} counterpart. This shift to higher energy is as expected because of the higher nuclear charge of Cu^{III} centers that makes it more difficult to excite a core electron.

Analysis of magnetic and absorption spectroscopic data[68] in conjunction with a number of theoretical studies[22, 29, 32, 78, 79] have led to a detailed picture of the bonding within the $Cu_2(\mu\text{-}O)_2$ core. Complexes with this core are diamagnetic, which is consistent with the d^8 electronic configuration of Cu^{III} and the tetragonal nature of the coordination sphere. In their optical absorption spectra, these complexes are characterized by two intense bands near 300 and 400 nm ($\varepsilon \sim 10\,000 - 25\,000\ M^{-1}cm^{-1}$). Attribution of the longer wavelength band to an oxo $\rightarrow$copper(III) CT transition is supported by its intensity and by resonance Raman excitation profiles, which show close correlation of the band shape for the 400 nm absorption with the ^{18}O-sensitive-band intensities in the Raman spectrum.[68] More detailed assignments of the absorption features, as well as other electronic structural insights, have come from computations that have defined the core bonding in molecular orbital (MO) terms. Two key frontier orbitals calculated for the model $[(NH_3)_6Cu_2(\mu\text{-}O)_2]^{2+}$ are shown in Figure 9;[22, 78] similar orbitals have been calculated for molecules with similar N-donor ligands at varying levels of theory.[68, 79] The filled, lower energy MO (Figure 9a) comprises oxygen p orbitals that are antibonding with respect to each other, but which have strong bonding interactions with the Cu $d_{x^2-y^2}$ orbitals (e.g. high covalency). Antibonding interactions between all of the metal and oxygen orbitals are present in the empty, higher lying MO (Figure 9b). Electronic excitation from the filled to the empty MO is thought to give rise to the lower energy optical transition ($\approx$400 nm),[68] with the intensity of this band arising from the high degree of metal–ligand bond covalency illustrated by the MO drawings. This large covalency also accounts for the strong enhancement observed for the Cu–O vibrations in resonance Raman spectra (Section 4). The higher energy UV absorption feature corresponds to one of similar energy and intensity found in (μ-η^2:η^2-peroxo)dicopper(II,II) units (peroxo $\pi^*_\sigma \rightarrow Cu\,d_{xy}$ LMCT)[80] and has been assigned analogously.[68]

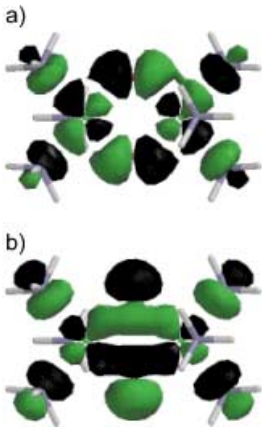

Figure 9. Key filled (a) and empty (b) frontier molecular orbitals calculated for $[(NH_3)_6Cu_2(\mu\text{-}O)_2]^{2+}$. Adapted with permission from ref. [11a].

Because Fe^{III} and Fe^{IV} centers can adopt different spin states, the electronic structures of the $Fe_2(\mu\text{-}O)_2$ complexes are more varied than those of their copper counterparts. The diiron(III) complexes with $Fe_2(\mu\text{-}O)_2$ and $Fe_2(\mu\text{-}O)(\mu\text{-}OH)$ cores characterized to date all have high-spin Fe^{III} ions and they exhibit electronic spectra similar to those of (μ-oxo)diiron(III,III) complexes. The latter compounds exhibit two moderately intense absorption features in the 500–700 nm region ($\varepsilon \approx 200 - 500\ M^{-1}cm^{-1}$) that have been assigned to transitions that have both LMCT and ligand-field character.[81, 82] Corresponding features for the $Fe_2(\mu\text{-}O)_2$ and $Fe_2(\mu\text{-}O)(\mu\text{-}OH)$ complexes are observed at 500 and 800 nm, with the latter band significantly red-shifted as a result of the acute Fe-O-Fe angles found in these cores.[43] Excitation into the 500 nm band gives rise to the core vibrations in the Raman spectra discussed in Section 4.

Like the (μ-oxo)diiron(III,III) complexes, the high-spin iron(III) centers in the $[Fe_2(\mu\text{-}O)_2]^{2+}$ and $[Fe_2(\mu\text{-}O)(\mu\text{-}OH)]^{3+}$ cores are antiferromagnetically coupled, but the strengths of the coupling interactions differ. Compounds with (μ-oxo)diiron(III,III) units have J values that range from 180 cm^{-1} to 250 cm^{-1} ($\mathbf{H} = J\mathbf{S_1}\mathbf{S_2}$) and that appear to be rather insensitive to Fe-O-Fe angles between 120° and 180°.[62] While introduction of a second efficient exchange pathway in complexes with $[Fe_2(\mu\text{-}O)_2]^{2+}$ and $[Fe_2(\mu\text{-}O)(\mu\text{-}OH)]^{3+}$ cores may lead to the expectation of an even stronger coupling interaction, these complexes actually exhibit weaker antiferromagnetic coupling. For example, $J = +110(10)\ cm^{-1}$ for $[(6\text{-}Me_3tpa)_2Fe_2(\mu\text{-}O)(\mu\text{-}OH)]^{3+}$ and $J = +54(8)\ cm^{-1}$ for $[(6\text{-}Me_3tpa)_2Fe_2(\mu\text{-}O)_2]^{2+}$.[42] These smaller J values have been ascribed to the rather small Fe-O-Fe angles (90–105°) and the longer Fe-μ-O bonds associated with these complexes. Indeed, the J values found for these complexes fit well into a published correlation that relates J values to the average Fe-μ-O bond length of the shortest superexchange pathway between two iron(III) ions.[83] The inclusion of data from these complexes refines and further validates this correlation by providing needed values for complexes with intermediate Fe–O bond lengths.

The electronic properties of the higher valent bis(μ-oxo)diiron(III,IV) complexes divide them into two subsets, depending on whether the iron ions are high or low spin. Those with high spin iron centers exhibit $S = ½$ ground states and have Mössbauer spectra consisting of two quadrupole doublets, one with an isomer shift δ of about 0.5 $mm\,s^{-1}$, characteristic of high-spin Fe^{III} centers, and the other with a δ value of around 0.1 $mm\,s^{-1}$, associated with Fe^{IV} centers (Table 4).[84] Consistent with the high-spin assignment, the hyperfine parameters of the Fe^{III} ion are isotropic, while those of the Fe^{IV} ion exhibit significant anisotropy. The $S = ½$ state thus must arise from the antiferromagnetic coupling of $S = 5/2$ Fe^{III} and $S = 2$ Fe^{IV} ions (Figure 10, left). Nine out of the ten d orbitals of the diiron(III,IV) center are magnetic, and superexchange causes antiparallel alignment, which can readily occur through single-atom bridges. The $S = ½$ spin state is also manifested in the EPR spectra as an isotropic signal at $g = 2$ at X-band frequency.[50, 51, 53, 54]

The other subset of bis(μ-oxo)diiron(III,IV) complexes consists of three closely related compounds with L = tpa, 5-Me_3-tpa, or 5-Et_3-tpa that have $S = 3/2$ ground states, as

Table 4. Mössbauer parameters for diiron(III,IV) complexes.

L or protein	Electronic description	$\delta(Fe^{IV})$	$\Delta E_Q(Fe^{IV})$	$\delta(Fe^{III})$	$\Delta E_Q(Fe^{III})$	Ref.
5-Me_3-tpa	valence delocalized $S=\frac{1}{2}$	0.14(2)	+0.49(3)	–	–	[48b]
6-Me_3-tpa	valence localized $S=\frac{1}{2}$	0.10	1.14	0.50	1.3	[51, 53]
6-Me-tpa	valence localized $S=\frac{1}{2}$	0.08(3)	0.5(1)	0.48	1.6(2)	[50]
$Ar^{Tol}CO_2$	valence localized $S=\frac{1}{2}$	0.12	0.6	0.55	1.1	[54]
RNR R2-**X**	valence localized $S=\frac{1}{2}$	0.26(4)	−0.6(1)	0.56(3)	−0.9(1)	[84a]
MMOH-$\mathbf{Q_X}$	valence localized $S=\frac{1}{2}$	0.14(6)	−0.6(1)	0.48(6)	−0.9(1)	[84b]

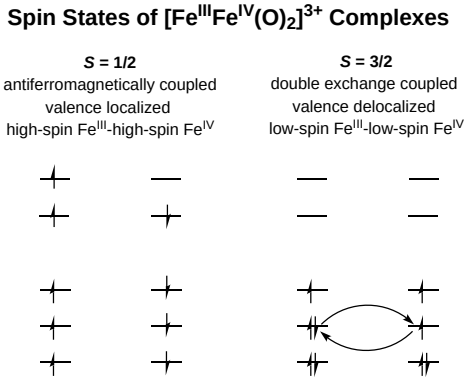

Figure 10. Overview of magnetic interactions and spin states in $[L_2Fe^{III}Fe^{IV}(O)_2]^{3+}$ complexes.

indicated by EPR spectra with g values at 4.3, 3.7, and 2.[48b] The metal ions in the $Fe_2(\mu\text{-}O)_2$ core supported by 5-Et_3-tpa were shown by X-ray crystallography to be in essentially equivalent environments.[49] Mössbauer spectra of the series of complexes consist of only one quadrupole doublet ($\delta \approx 0.14\,mm\,s^{-1}$) showing that the $Fe^{III}Fe^{IV}$ center is valence delocalized.[48] The $S=\frac{1}{2}$ ground state derives from the parallel alignment of the single spin on the $S=\frac{1}{2}$ Fe^{III} center and the two spins of the $S=1$ Fe^{IV} ions that is enforced by a double exchange mechanism (Figure 10, right).

Density functional theory (DFT) calculations have provided an MO description that rationalizes the observed $S=\frac{1}{2}$ ground state.[85] As shown in Figure 11, the frontier MOs of $[Fe_2(\mu\text{-}O)_2(tpa)_2]^{3+}$ with predominant metal 3d character consist of two groups well separated in energy. The low-energy set comprises six MOs derived from various combinations of the metal t_{2g} orbitals. Filling these six MOs with nine 3d electrons following Hund's rule results in the observed $S=\frac{1}{2}$ ground state, consistent with the low-spin description implied by the experimental data. Mulliken analysis of the unpaired spin populations show that the three unpaired electrons are fully localized on the $[Fe_2(\mu\text{-}O)_2]^{3+}$ core and are distributed between the iron and the oxygen atoms in a 4:1 ratio. The fact that neither the iron nor the oxygen atoms have integral spin populations indicates significant covalency in the bonding within the $[Fe_2(\mu\text{-}O)_2]^{3+}$ unit.

The valence delocalized $[L_2Fe_2(\mu\text{-}O)_2]^{3+}$ complexes were first observed because of their characteristic green color arising from an intense visible absorption band at 616 nm ($\varepsilon \sim 5000\,M^{-1}\,cm^{-1}$).[48] Since oxo→iron CT transitions for oxo-bridged diiron complexes are usually found in the near UV region,[81, 82] such an intense band at low energy is atypical and hinted at the unusual valence delocalized electronic structure

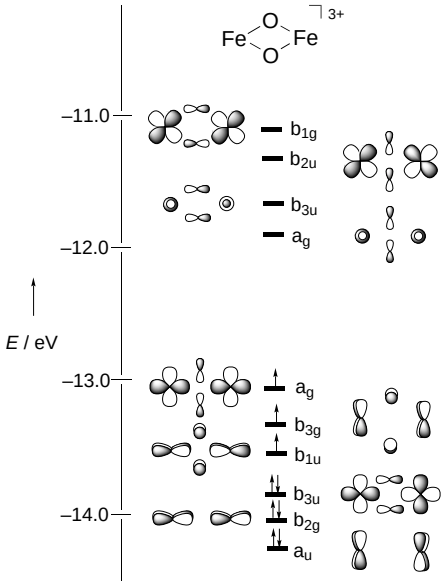

Figure 11. Frontier molecular orbitals of the $S=\frac{1}{2}$ $[Fe_2(\mu\text{-}O)_2]^{3+}$ core, with the indicated irreducible representations indicated for the D_{2h} point group. Adapted with permission from ref. [85].

that was subsequently established. The sharpness of this band and its insensitivity to solvent argue against a LMCT designation and support its assignment as an intervalence (metal-to-metal) transition.[48b]

To summarize, the parent tpa ligand and its two 5-alkyl substituted derivatives give rise to valence delocalized $S=\frac{1}{2}$ complexes, while its two 6-methyl substituted derivatives form valence trapped $S=\frac{1}{2}$ complexes. It is remarkable how the introduction of one 6-methyl group can so dramatically alter the electronic structure of the $[Fe_2(\mu\text{-}O)_2]^{3+}$ core.[51] Clearly, these results emphasize the important influence of ligand structural features on the physical properties of such metal centers.

6. Reactivity

Two major modes of reactivity are exhibited by the thermally unstable bis(μ-oxo)dicopper and/or -diiron complexes: a) core isomerization, which involves O–O bond formation in a conversion into a μ-η^2:η^2-peroxo core (Cu) or bridge-to-terminal oxo migration (Fe), and b) oxidation of organic functional groups, in either intra- or intermolecular processes. The core isomerization and hydrocarbon C–H activation reactions are of fundamental importance in oxida-

tions performed by non-heme enzymes or synthetic catalysts, and as a result much effort has been expended to understand associated mechanistic issues.

6.1. Core Isomerization

The separate isolation of μ-η^2:η^2-peroxo- and bis(μ-oxo)dicopper complexes with different supporting N-donor ligands (e.g., $Tp^{R,R'}$ versus Bn_3tacn; Tp = tris(pyrazolyl)hydroborate) suggested that under suitable conditions these two isomeric cores might interconvert in an unprecedented process. Studies of the oxygenation of Cu^I complexes of iPr$_3$tacn a) led to the identification of both peroxo and bis(μ-oxo) isomers supported by the same N-donor ligand and b) provided the first experimental evidence that these particular isomers could indeed participate in a facile equilibrium.[11, 21] Important evidence included the identification by UV/Vis and resonance Raman spectroscopy of $[(i\text{Pr}_3\text{tacn})_2\text{Cu}_2(\mu\text{-}\eta^2\text{:}\eta^2\text{-}O_2)]^{2+}$ upon performing the low-temperature oxygenation of $[(i\text{Pr}_3\text{tacn})\text{Cu}(CH_3CN)]^+$ in CH_2Cl_2 and the finding of spectral features arising from the bis(μ-oxo) core when the oxygenation was performed in concentrated THF solutions. Solvent-mixing experiments involving dilution of concentrated CH_2Cl_2 solutions with THF and vice versa resulted in spectral changes indicating transmutation of the isomers.[21, 39] In acetone, spectral signatures of both forms were seen. These initial discoveries showed that the two cores supported by iPr$_3$tacn have similar thermodynamic stabilities, such that changes in solvent are sufficient to result in formation of one or the other form. Consistent with the energetic similarity between the isomers, X-ray diffraction and resonance Raman spectroscopic data obtained on crystals isolated from CH_2Cl_2 solution suggested the existence of both forms, compositionally disordered, in the solid state.[11]

Evidence for a rapid isomerization equilibrium between the compounds supported by iPr$_3$tacn came from the results of low-temperature stopped-flow kinetics experiments.[21] The formation of a $\approx$4:1 mixture of the peroxo and bis(μ-oxo) isomers from the reaction of $[\text{LCu}(CH_3CN)]^+$ with O_2 in acetone was found to have a first-order dependence on the concentration of the Cu^I complex. Activation parameters (Table 2) are consistent with formation of $[\text{LCu}(O_2)]^+$ in the rate-determining step. In addition, the spectral features of each isomer grew at identical rates at a range of temperatures ($-83\,^\circ$C to $-50\,^\circ$C). Identical rates of decomposition because of intramolecular C–H bond activation (Section 6.2) also were observed. These findings are best rationalized by the involvement of an equilibrium between the isomers that is more rapid than the 1:1 $Cu-O_2$ adduct formation or decomposition steps (Scheme 1). The results of a recent detailed study of the solvent and temperature dependence of the ratio of the isomers are consistent with this equilibrium, and yield thermodynamic parameters for solutions in THF of $\Delta H = 4\ \text{kJ mol}^{-1}$ and $\Delta S = 25\ \text{J mol}^{-1}\ \text{K}^{-1}$.[39]

Subsequent to the discovery of the peroxo/bis(μ-oxo) equilibrium in the system with iPr$_3$tacn, evidence for similar equilibria in systems supported by other ligands has been reported.[27, 28, 30, 33] On the basis of UV/Vis, resonance Raman, and X-ray absorption spectroscopic data (X-ray absorption near-edge spectroscopy (XANES) and EXAFS) it was shown that oxygenation of $[(\text{MePy2})\text{Cu}]^+$ yields a mixture of μ-η^2:η^2-peroxo- and bis(μ-oxo)dicopper isomers in solution (CH_2Cl_2) and in the solid state (ratio $\approx$4:1).[28] Stopped-flow kinetic data were found to be consistent with a rapid equilibrium between the isomers. In addition, a compositionally disordered X-ray crystal structure akin to the one obtained for the system comprising iPr$_3$tacn was obtained. Interestingly, only the peroxo core was observed (UV/Vis, Raman) for the system supported by $PhCH_2CH_2$Py2, which differs from MePy2 only with respect to the alkyl substituent.[40] Kinetics data for the decay of this μ-η^2:η^2-peroxo complex suggested that isomerization to a bis(μ-oxo) core occurs prior to intramolecular C–H bond activation (see Section 6.2). Isomerization of the bis(μ-oxo)dicopper unit supported by 6-Me$_2$tpa to a μ-η^2:η^2-peroxo core was implicated by the observation of reversibility in the oxygenation process.[30] Thus, bubbling N_2 through a solution of $[(6\text{-Me}_2\text{tpa})_2\text{Cu}_2(\mu\text{-}O)_2]^{2+}$ in CH_2Cl_2 at $-80\,^\circ$C or addition of PPh_3 to a solution in acetone caused ejection of O_2 and formation of monomeric Cu^I species, presumably via a peroxo intermediate which was not observed. More recently, mixtures of peroxo and bis(μ-oxo) isomers were observed upon oxygenation of Cu^I complexes of a range of peralkylated diamine ligands $R^1_2R^2_2$eda and $R^1_2R^2_2$pda, with equilibrium constants that were sensitive to the ligand structure, solvent, counterions, and temperature.[33] Interestingly, and in contrast to all other cases, for the system with L = tBu$_2$Me$_2$eda in MeTHF solvent, isomer interconversion was slow relative to decomposition, and differential reactivity of the two isomers both with respect to decay and to oxidations of added substrates was observed.

Taken together, the data indicating the existence of the peroxo/bis(μ-oxo) equilibrium with a range of N-donor ligands point to the potential general significance of the isomerization process in reactions that involve the making or breaking of the dioxygen O–O bond. We note that no examples of the (μ-η^2:η^2-peroxo)diiron or -dimanganese core have been identified in synthetic complexes or in biological systems. Nonetheless, and despite theoretical arguments to the contrary,[86] it remains conceivable that such species may be involved as intermediates in bis(μ-oxo)dimetal complex generation through an O–O bond breaking process (or the opposite) now with a precedent in copper-containing systems.

The finding of either or both isomeric cores in copper complexes with divergent ligands raises questions concerning what ligand structural features are the most important in controlling which isomer predominates. Examination of the existing data suggests some general rules: bis(μ-oxo) complex formation is favored when the supporting ligand a) is bidentate, b) has strongly σ-donating amine donors, c) is less sterically hindered (smaller N-donor ligand substituents), and/or d) has a constraining tether between donor portions (e.g., iPr$_4$dtne). These features may be understood in an intuitive way by considering the core shapes and formal oxidation states of the copper ions in the two forms. There is a long distance ($\approx$3.5 Å) between Cu^{II} ions in the peroxo isomer versus a short distance ($\approx$2.8 Å) between more

electron deficient Cu^{III} ions in the bis(μ-oxo) form. Thus, strongly electron-donating ligands that best enable (or only allow) a short intermetal separation and a square-planar coordination geometry favorable to d^8 Cu^{III} centers tend to support bis(μ-oxo) core formation. Conversely, tridentate ligands with sterically encumbered substituents or spacers that inhibit close approach of the metal ions and/or poorer electron donors tend to favor the (μ-η^2:η^2-peroxo)dicopper(II,II) core. It has been suggested that another factor is the N_{eq}-Cu-N_{eq} bite angle; the smaller the angle, the greater the stability of the bis(μ-oxo) form that is characterized by more acute Cu-O-Cu and correspondingly more obtuse O-Cu-O angles than the peroxo isomer.[28] This simple angular dependence was evaluated by a theoretical analysis of $[(NH_3)_4Cu_2(\mu\text{-}O)_2]^{2+}$ units and was suggested to arise from differences in the energetics of the interactions between Cu and O orbitals in the two forms.[28]

Particularly subtle effects come into play when comparing systems that have identical donor sets. For example, oxygenation of [(*i*Pr$_3$tacd)Cu(CH$_3$CN)]$^+$ in CH_2Cl_2, THF, or acetone yields only the peroxo core, in contrast to the aforementioned behavior of the iPr$_3$tacn system (both isomers accessible) that differs only with respect to the deletion of a single -CH_2- group within the macrocycle.[29] A comparative analysis of the X-ray structures of the Cu^I precursors supported by these two ligands, in conjunction with integrated molecular orbital/molecular mechanics calculations on the complete peroxo and bis(μ-oxo) complexes, showed that the steric clashes between the *i*Pr groups in the bis(μ-oxo) form are enhanced for the case of the larger tacd macrocycle. These clashes ultimately result in a relative quantum mechanical destabilization of the bis(μ-oxo) core that is manifested in sole experimental observation of the other (peroxo) form. Similar steric effects were invoked to explain differences in the equilibrium constants between peroxo and bis(μ-oxo) forms with bidentate peralkylated amine ligands $R^1_2R^2_2$eda and $R^1_2R^2_2$pda, with larger K_{eq} = [peroxo]/[bis(μ-oxo)] for systems supported by ligands with the same backbone but larger substituents (Me$_2$*i*Pr$_2$pda > Me$_4$pda) and with larger backbones and the same substituents (e.g. Me$_2$*i*Pr$_2$pda > Me$_2$*i*Pr$_2$eda).[33]

The μ-η^2:η^2-peroxo/bis(μ-oxo) equilibration has not been observed in diiron systems, although the possibility of such a conversion has been raised in calculations of mechanisms postulated for methane monooxygenase (MMO) catalysis to account for the formation of the Fe_2O_2 core of intermediate **Q**.[87] The synthetic (peroxo)diiron(III,III) intermediates reported to date do not contain the μ-η^2:η^2-peroxo unit, but instead are of the μ-1,2-peroxo type (Scheme 3), and most retain their structural integrity at the temperatures at which they are characterized.[12b, 18d] X-ray crystal structures of three such (peroxo)diiron(III,III) complexes are known.[88] Subsequent decomposition by raising the temperature has usually afforded no other discernible intermediate species prior to the formation of diiron(III,III)) or polyiron(III) decay products. In one example, however, a (μ-oxo)(μ-1,2-peroxo)diiron(III,III) species derived from either the reaction of O_2 with $[(6\text{-}Me_3tpa)_2Fe_2(\mu\text{-}OH)_2]^{2+}$ or H_2O_2 with $[Fe_2(\mu\text{-}O)_2(6\text{-}Me_3tpa)_2]^{2+}$ converted in moderate yield into a high-valent species minimally formulated as $[(6\text{-}Me_3tpa)_2Fe_2(O)_2]^{3+}$.[51, 52] The mechanism of the conversion of the peroxo to the high-valent oxo complex is still not established.

Core isomerization of a different type has been implicated by the results of studies of the oxidation of the bis(μ-oxo)-diiron(III,III) complex supported by 6-Me$_3$tpa (Scheme 7).[53] Addition of $(NBu_4)_2[Ce(NO_3)_6]$ to a solution of the complex in CH_3CN at $-40\,^\circ C$ (characterized by $E_{1/2} = 0.41$ V versus ferrocene) afforded in high yield a species that was formulated as $[(6\text{-}Me_3tpa)_2Fe_2(O)_2(H_2O)]^{3+}$ on the basis of elemental analysis and ESI-MS data. The two oxygen atoms in the complex were found to be distinct on the basis of their different rates of exchange with isotopically labeled H_2O as revealed by resonance Raman spectroscopy. In the resonance Raman spectrum, a feature at 840 cm^{-1} was attributed to the ν_{Fe-O} of a terminal Fe^{IV}=O unit that was not prone to solvent water exchange, with a small contribution from the ν_{asym} of an Fe-O-Fe unit that does exchange with water. In corroboration of this structural hypothesis, EXAFS spectra of the oxidized species show that the outer-sphere scattering between the Fe atoms characteristic for the diamond $Fe_2(\mu\text{-}O)_2$ core is absent.[89] A nearly isotropic signal with $g = 1.999$ in the EPR spectrum in conjunction with Mössbauer data indicate that the system contains a $Fe^{III}Fe^{IV}$ pair with $S = ½$. Taken together, the evidence supports the structure shown in Scheme 7 with an Fe^{III} center linked by an oxo bridge to a Fe^{IV}=O moiety. The overall conversion from a bis(μ-oxo)diiron(III,III) complex into this product involves a coupled one-electron oxidation and bridge-to-terminal oxo migration, which suggests a flexibility of the bis(μ-oxo)diiron motif that may be of biological and catalytic significance.

6.2. Oxidations

The bis(μ-oxo)dicopper and -diiron complexes isolated so far are capable of oxidizing various organic functionalities in reactions of biological relevance, and in several cases mechanistic information is available. In general, the copper compounds are one or two-electron oxidants, whereas the iron species mainly perform one-electron oxidations.

Best studied are the ubiquitous decomposition reactions of the bis(μ-oxo)dicopper compounds, which generally proceed by attack of the C–H bonds of a supporting-ligand substituent by the oxidizing core. As illustrated for the R$_3$tacn system in Scheme 9, C–H bonds α to an N donor of the supporting ligand are the most common targets in these reactions. The final products are bis(μ-hydroxo)dicopper(II,II) compounds, which in several cases were shown to contain capping ligands in which an N–R group of the original ligand is replaced by an N–H moiety.[22] The overall N-dealkylation reaction was quantified by removal of the copper ions from the product mixture and identification of the resulting organic products by NMR spectroscopic and gas chromatography (GC)/MS methods. An intramolecular pathway was shown to be operative on the basis of a) observed kinetics that uniformly are first-order in the bis(μ-oxo)dicopper complex concentration and b) a classical double-labeling experiment in which benzaldehyde product was analyzed upon allowing a mixture of

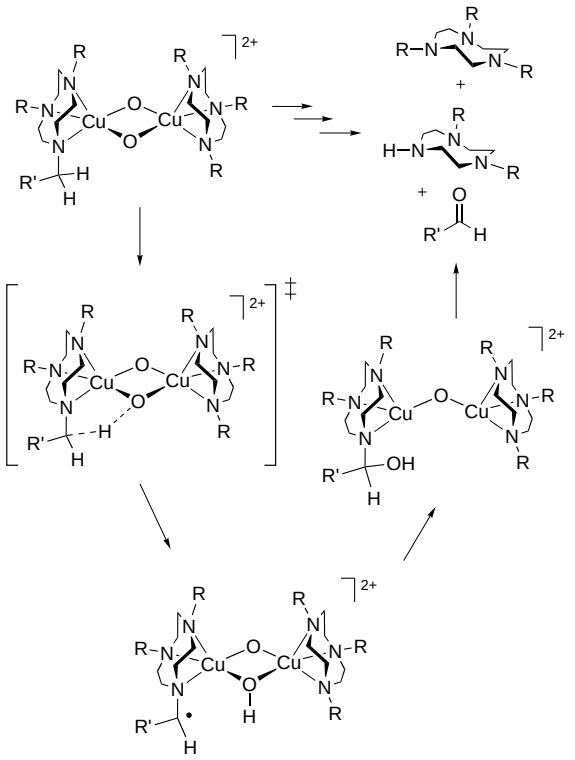

Scheme 9. Oxidative N-dealkylation reaction with postulated mechanism for an illustrative bis(μ-oxo)dicopper complex. R = R′CH_2, where R′ = alkyl and or aryl groups (see Table 5 for kinetic data).

$[(Bn_3tacn)_2Cu_2(^{16}O)_2]^{2+}$ and $[(Bn'_3tacn)_2Cu_2(^{18}O)_2]^{2+}$ (Bn′ = 4-*tert*-butylbenzyl) to decompose.[90] Comparison of activation parameters (Table 5) reveals a general similarity across an array of systems, with negative $\Delta S^{\neq}$ values consistent with an ordered transition state. Importantly, large H/D kinetic isotope effects (KIEs) were uncovered that indicate C–H(D) bond scission in the rate-determining step. Indeed, the magnitude of these KIE values and their temperature dependencies implicate a tunneling contribution akin to that seen in several biological oxidations.[91, 92] Finally, a plot of the rate constants for the series of complexes supported by (X-Bn)$_3$tacn (X = MeO, Me, *t*Bu, H, CO_2Me, and CF_3) versus σ^+ values yielded $\rho = -0.4$,[93] a small negative value similar to those measured for H-atom abstractions by electrophilic radical reagents and heme–iron oxidants.[94]

Taken together, the experimental evidence is consistent with a mechanism for the N-dealkylation reaction (Scheme 9) that involves rate-controlling attack of the bridging oxo unit on the α C–H bond, either by H-atom abstraction or a concerted insertion process (not shown).[90] For the former, the resulting radical would be trapped by internal OH· transfer in a fast "rebound" step[2] to yield the same intermediate carbinolamine that would result from the latter direct insertion. Fast N-dealkylation of the carbinolamine intermediate would yield the final carbonyl fragment and amine. The available experimental data does not allow distinction between the "rebound" and "direct insertion" routes, a dichotomy that parallels that which is under debate for oxidations mediated by heme and non-heme iron enzymes.[95] It is noteworthy that recent calculations on the complete system supported by Bn$_3$tacn using a integrated molecular orbital/molecular mechanics method yielded a transition state for the rate-determining step that is consistent with H-atom abstraction (Figure 12), with reasonable agreement between the calculated and experimentally determined kinetic parameters.[96]

Table 5. Selected activation parameters and H/D kinetic isotope effects (KIE) for decomposition reactions of $[Cu_2(\mu\text{-}O)_2]^{2+}$ complexes.

Supporting ligand	$\Delta H^{\neq}$ [kJ mol^{-1}][a]	$\Delta S^{\neq}$ [J mol^{-1} K^{-1}][a]	H/D KIE (T [°C])	Ref.
Me_3tacn	53(1)	−75(12)	–	[26]
*i*Pr$_3$tacn	55(2)	−59(8)	26 (−40)	[90]
Bn$_3$tacn	54(2)	−54(8)	40 (-40)	[90]
R$_3$tacn (n = 2)[b]	60	−23	–	[31]
R$_3$tacn (n = 3)[b]	62	−39	–	[31]
Me_3TACD	51(2)	−100(8)	–	[29]
*i*Pr$_4$dtne	56(2)	−59(8)	40 (−40)	[23]
*i*Pr$_4$-*m*-XY[c]	31(1)	−151(5)	–	[24]
*i*Pr$_4$-*p*-XY[c]	38(2)	−108(7)	–	[24]
Et_2Me_2chd	49(1)	−105(4)	[d]	[26]
Me_4chd	56(1)	−100(4)	–	[26]
EtPhPy	39.1(4)	−73(2)	35 (−80)	[27]

[a] Approximate estimated error in the measured value is indicated in parenthesis. [b] R$_3$tacn refers to tacn ligand with aryl ether dendrimer substituents, with n = number of aromatic layers of dendron subunits. [c] Data reported for k_6, the first of two consecutive rate constants that characterize the decay of the complexes that contain two $[Cu_2(\mu\text{-}O)_2]^{2+}$ units. [d] A KIE value of 3.0 (extrapolated to 20 °C) was measured by using ligand deuterated only at the ethyl groups to obtain a "k_D". However, because involvement of C–H bond attack at the nondeuterated Me groups in this Et-deuterated ligand was not conclusively ruled out, this value may not necessarily reflect the actual KIE.

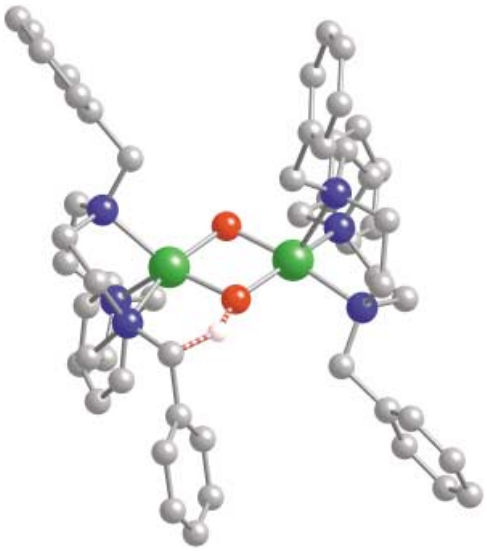

Figure 12. Structure of the transition state for the C–H bond breaking step of the N-dealkylation reaction of $[(Bn_3tacn)_2Cu_2(\mu\text{-}O)_2]^{2+}$ as determined from integrated molecular orbital/molecular mechanics calculations.[96]

The H-atom abstraction reactivity that is implicated in the well-studied N-dealkylation pathway of the bis(μ-oxo)dicopper core also is manifested in oxidations involving other types of C–H bonds in ligand substituents and external reagents, as well as heteroatom X–H (X = O or S) bonds in phenols or

thiophenols. For example, intramolecular benzylic hydroxylation occurs upon decomposition of $[(EtPhPy)_2Cu_2(\mu\text{-}O)_2]^{2+}$ (Scheme 10).[27] On the basis of kinetic studies that enabled determination of activation parameters (Table 5) and a Hammett ρ value (-1.48, by varying the X group) similar to

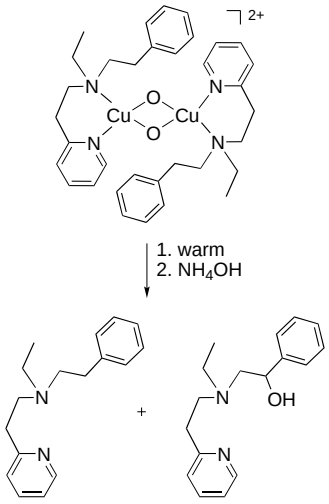

Scheme 10. Intramolecular benzylic hydroxylation observed upon decomposition of the bis(μ-oxo)dicopper complex of EtPhPy.[26]

those observed in the N-dealkylations, a mechanism directly analogous to the one postulated for the N-dealkylations was proposed. In this instance, however, the product resulting after "rebound" is a stable alcohol. A similar benzylic hydroxylation occurs for the system supported by $PhCH_2CH_2Py2$, but a μ-η^2:η^2-peroxo $\rightarrow$bis(μ-oxo) conversion was proposed to be rate limiting (instead of C–H bond attack).[40] Stereoselective hydroxylations of prochiral substituents in copper systems supported by other RPy2 ligands also have been reported, although direct evidence for involvement of a bis(μ-oxo)dicopper intermediate was not provided.[97]

Conversion of phenols into phenoxyl radicals is a general reaction of bis(μ-oxo)dicopper complexes, which yields coupled products or directly observable radicals depending on the substituent pattern of the phenol used. Formation of (μ-hydroxo)dicopper(II,II) species as coproduct has been observed for the Cu systems.[20] Oxidation of catechols also is commonly observed for dicopper systems,[34, 98] although the nature of the product isolated depends on the supporting N-donor ligand (Scheme 11). Thus, with Me_4pda complexes *ortho*-quinone formation was observed, but with R_3tacn derivatives, Cu^{II}-semiquinonato complexes were generated. Other interesting contrasts have been observed in the reactions of bis(μ-oxo)dicopper complexes of Me_4pda and R_3tacn that have been suggested to arise from differences in the accessibility of the core to external reagents.[34] Of particular note is the unique capability of the Me_4pda complex to oxidize alcohols to aldehydes or ketones and benzylamine to benzonitrile. Binding of substrate to the Cu^{III} center(s) in this complex as a first step is implicated from preliminary

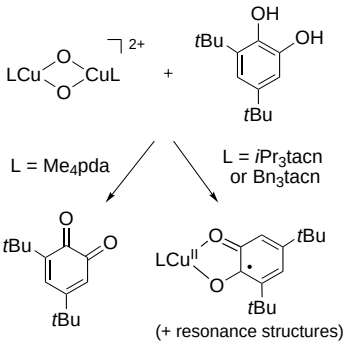

Scheme 11. Differences in reactivity of bis(μ-oxo)dicopper complexes with catechols.[34, 98]

mechanistic studies. Corroborating the ability of the metal centers to coordinate exogenous ligands, EXAFS results have been interpreted to suggest that a perchlorate anion bridges the core.[34]

There are also a few instances of intermolecular H-atom abstraction by $[Cu_2(\mu\text{-}O)_2]^{2+}$ complexes from weak aliphatic C–H bonds such as those of cyclohexadiene or dihydroanthracene.[35, 36] One study involves a system with a rapid $Cu_2(\mu$-η^2:η^2-$O_2)/Cu_2(\mu\text{-}O)_2$ equilibrium, so it is not clearly established precisely which moiety is responsible for the H-atom abstraction event.[28, 35] In another study where the $[Cu_2(\mu\text{-}O)_2]^{2+}$ isomer is clearly the only one present, H-atom abstraction of 10-methyl-9,10-dihydroacridine was observed.[36] Interestingly, the observed rate law has a second-order dependence on the concentration of the bis(μ-oxo) complex. This unusual kinetic behavior requires either a ternary transition state or conproportionation of the $[Cu_2(\mu\text{-}O)_2]^{2+}$ core to form an even more highly oxidized species that is responsible for the subsequent H-atom abstraction. These examples demonstrate that some of the mechanistic intricacies with respect to H-atom abstraction by $Cu_2(\mu\text{-}O)_2$ complexes remain to be unraveled.

Another unresolved mechanistic issue concerns the nature of the copper/oxygen species responsible for arene hydroxylations in biological and synthetic systems.[10b] For example, while a μ-η^2:η^2-peroxo unit has been identified in tyrosinase[3d] and catechol oxidase,[3g, 99] the observation of the peroxo/bis(μ-oxo) equilibration in synthetic compounds implicates its possible occurence in the enzyme mechanisms, and raises the possibility that a bis(μ-oxo) intermediate (yet to be observed directly) may in fact be the oxidizing species during enzymatic catalysis. Intra-[11b, 18] and intermolecular[100] arene hydroxylations have been observed upon decay of several (peroxo)dicopper complexes, and evidence has been presented that argues against the intermediacy of a bis(μ-oxo) isomer.[101] Although H-atom abstraction has been the predominantly observed reaction for bis(μ-oxo)dicopper complexes, arene hydroxylation was seen when the $[Cu_2(\mu\text{-}O)_2]^{2+}$ core supported by $ArPyNEt_2$ decomposed (Scheme 12).[25] Rate-controlling electrophilic attack at the aromatic π system was supported by the observation of lower rates of decay for derivatives with electron withdrawing groups on the arene and the absence of a rate effect when the ring was perdeuterated. Although these results provide important

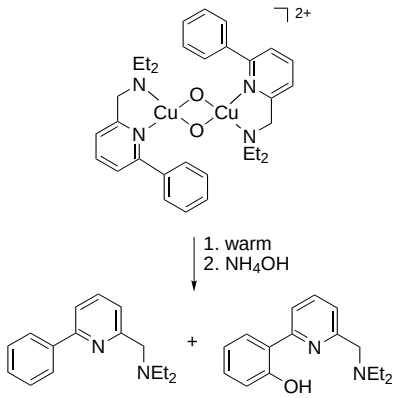

Scheme 12. Aromatic hydroxylation observed upon decomposition of the bis(μ-oxo)dicopper complex of $ArPyNEt_2$.[25]

precedent for the possible involvement of the $[Cu_2(\mu\text{-}O)_2]^{2+}$ core in aromatic hydroxylations, fast pre-equilibration with a trace, but unobserved, amount of a reactive peroxo isomer cannot be ruled out. Thus, conclusive proof that the bis(μ-oxo)dicopper unit is capable of aromatic hydroxylation has yet to be obtained.

Like their dicopper(III,III) counterparts, the bis(μ-oxo)diiron(III,IV) complexes also carry out H-atom abstraction reactions. All three types of such compounds ($S = 3/2$ with tpa, $S = 1/2$ with 6-Me_3tpa, and $S = 1/2$ with $ArCO_2^-$) quantitatively oxidize 2,4-di-*tert*-butylphenol to the corresponding biphenol via a phenoxyl radical intermediate (Scheme 13a).[52, 54, 102] The two tpa complexes are reduced to (μ-oxo)diiron(III,III) complexes, so the phenol $\rightarrow$phenoxyl radical reactions mimic the key step in the formation of the active diiron(III,III)-tyrosyl radical cofactor of ribonucleotide reductase.[3c]

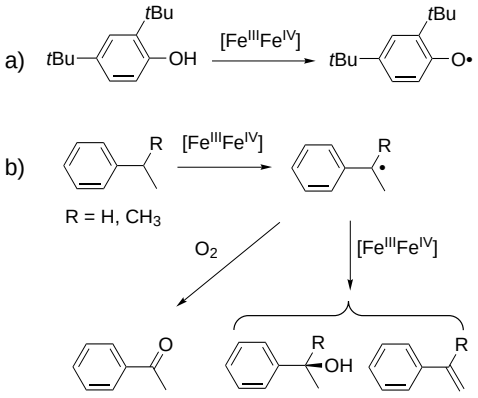

Scheme 13. Reactivity of $Fe^{III}Fe^{IV}$ complexes with a phenol (a)[52, 54, 102] and hydrocarbons (b).[102]

Oxidations more relevant to the catalytic chemistry of MMO and fatty acid desaturases have thus far been investigated only for $[(tpa)_2Fe_2(\mu\text{-}O)_2]^{3+}$.[102] This complex reacts with hydrocarbons such as ethylbenzene and cumene to afford products that correspond to the hydroxylation of the benzylic carbon or the dehydrogenation of the α- and β-CH bonds (Scheme 13b), conversions analogous to those catalyzed by MMO and fatty acid desaturases, respectively.[3a,b, 12] The stoichiometry for these reactions requires the consumption of two molecules of $[(tpa)_2Fe_2(\mu\text{-}O)_2]^{3+}$ per molecule of product formed. Thus, unlike the diiron sites of the enzymes which effect two-electron oxidations of the substrate, the synthetic diiron(III,IV) complex is a one-electron oxidant. Furthermore, it can only cleave benzylic C–H bonds, not the unactivated C–H bonds that are typical of substrates for the above enzymes. Perhaps not surprisingly, the oxidizing power of the bis(μ-oxo)diiron(III,IV) core appears to be considerably less than that of the diiron(IV,IV) center generated in the MMO reaction cycle and presumed to be formed in the catalytic cycle of the fatty acid desaturases.[3a]

Mechanistic studies of the C–H bond cleavage reactions have provided revealing insights.[102] The kinetics of ethylbenzene oxidation at $-40\,^{\circ}C$ monitored by the disappearance of the green chromophore associated with $[(tpa)_2Fe_2(\mu\text{-}O)_2]^{3+}$ showed that the reaction is first order in substrate and in the dinuclear complex (second order overall) and exhibits a large KIE value of 20. This value was corroborated by measurement of the relative amounts of protio- and deutero-products, which yielded KIE values of 22 for phenethyl alcohol formation and 28 for styrene formation. These product isotope effects show that the cleavage of the α-C–H bond is a major component of the rate-determining step for both hydroxylation and desaturation of ethylbenzene, and the larger number for styrene formation reflects the additional isotope effect (ca. 1.3) arising from the cleavage of the β–H bond of ethylbenzene. These data are consistent with a rate-determining H-atom abstraction to generate an intermediate benzylic radical, which then reacts with a second equivalent of $[(tpa)_2Fe_2(\mu\text{-}O)_2]^{3+}$ to form either the C–O bond of the alcohol product or lose a β-hydrogen en route to styrene. These second steps are relatively slow as the intermediate radical can be intercepted by O_2 to afford products derived from the decomposition of alkylperoxy radicals, for example, acetophenone. These results show that, while the isolation and characterization of a bis(μ-oxo)iron(III)iron(IV) complex represented an important step forward in establishing the viability of an $Fe_2(\mu\text{-}O)_2$ diamond core in non-heme iron oxidation chemistry, there is still more to be accomplished in biomimetic efforts, not the least of which is the generation and study of the reactivity of a bis(μ-oxo)diiron(IV,IV) species that would correspond to MMO intermediate **Q** (see addendum).

Finally, recent studies of bis(μ-oxo)dinickel and -cobalt complexes have shown that the oxidizing capability of the $M_2(\mu\text{-}O)_2$ unit is not limited to M = Cu and Fe.[14–16] Decomposition of $[(Tp^{Me3})_2M_2(\mu\text{-}O)_2]$ (M = Ni or Co) and $[(6\text{-}Me_3tpa)_2Ni_2(\mu\text{-}O)_2]^{2+}$ resulted in oxidation of either a supporting ligand methyl group to its respective alcohol or N-dealkylation.[14, 15] An H-atom abstraction pathway was implicated by a further functionalization of the ligand of the $[(6\text{-}Me_3tpa)_2Ni_2(\mu\text{-}O)_2]^{2+}$ complex to yield a carboxylate group when the reaction was performed under an O_2 atmosphere. Consistent with this H-abstraction mode of reactivity, the 6-Me_3tpa-supported dinickel complex also effectively couples 2,6-di-*tert*-butylphenol. Similar reactivity with phenols was manifested by $[(EtPhPy)_2Ni_2(\mu\text{-}O)_2]^{2+}$.[16] In addition, the decomposition of this compound in the absence of added substrate resulted in benzylic hydroxylation of the

supporting EtPhPy ligand in a process shown by mechanistic studies to involve rate-determining benzylic H-atom abstraction much like that observed for the bis(μ-oxo)dicopper analogue.[40] In sum, the high-valent bis(μ-oxo)dimetal complexes of the later first row transition series generally display similar reactivity, most notably involving substrate oxidation by H-atom abstraction pathways.

7. Relevance to Metalloenzymes

High-valent metal centers with M_2O_2 diamond cores figure prominently in oxygen activation mechanisms currently proposed for non-heme enzymes with bimetallic active sites (Figure 13).[3, 6, 11, 12] These mechanisms follow the well-established heme paradigm, wherein an iron(II) porphyrin center

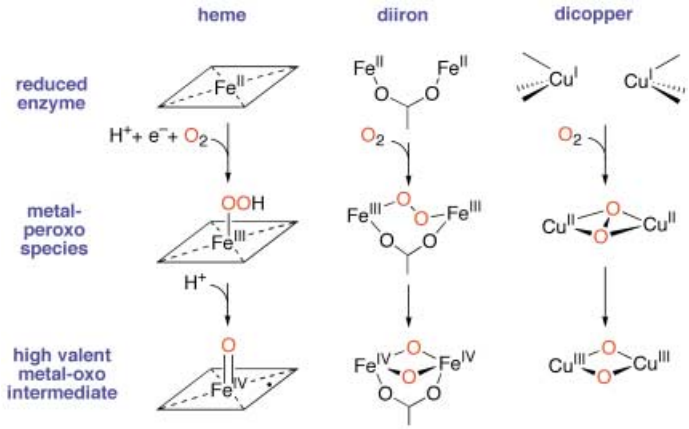

Figure 13. Unified scheme for dioxygen activation in the catalytic cycles of heme – iron and non-heme – diiron and –dicopper enzymes.

binds O_2, picks up an electron and a proton to form a hydroperoxoiron(III) intermediate, and then undergoes O–O bond cleavage to afford an oxoiron(IV) porphyrin radical species that is primarily responsible for the oxidation of substrates.[2] In the dinuclear context, the corresponding intermediates are a peroxo-bridged dimetal unit and a high-valent $M_2(\mu\text{-}O)_2$ species. Notably, a firm experimental basis for the notion that the latter may be involved in biological oxygen activation has been provided by the synthesis and characterization of synthetic complexes that contain the $M_2(\mu\text{-}O)_2$ core.

Although intermediates with the isomeric $[Cu_2(\mu\text{-}\eta^2\text{:}\eta^2\text{-}O_2)]^{2+}$ core[58] have been identified for the metalloproteins hemocyanin, tyrosinase, and catechol oxidase,[3d,f,g, 60] direct spectroscopic evidence for an enzyme species with the isomeric $[Cu_2(\mu\text{-}O)_2]^{2+}$ core is not yet available. Nevertheless, the demonstration in some synthetic complexes of a facile equilibrium between these two cores lends support to the postulate of a $[Cu_2(\mu\text{-}O)_2]^{2+}$ species as a possible reactive intermediate. Certainly the observation of an intramolecular oxygen-atom transfer, in a synthetic $[Cu_2(\mu\text{-}O)_2]^{2+}$ complex, to a pendant arene on the ligand[11b, 25] serves as a reasonable model for tyrosinase chemistry and makes the proposed involvement of a $Cu_2(\mu\text{-}O)_2$ core plausible.[103]

In non-heme iron chemistry, the availability of complexes with $Fe_2(\mu\text{-}O)_2$ cores led to the design of experiments that shed light on the diiron core structure of high-valent intermediate **Q** of methane monooxygenase (MMOH-**Q**). EXAFS analysis of MMOH-**Q** showed that the diiron(IV,IV) core has an Fe–Fe distance of 2.5 Å.[51] This rather short metal – metal distance is unique and requires the presence of at least two single-atom bridges with short metal – ligand bonds, attributes easily accommodated by the oxo bridges of an $M_2(\mu\text{-}O)_2$ core. Since the metal – metal distances in synthetic $M_2(\mu\text{-}O)_2$ complexes (Table 3) are minimally (0.2 Å) longer than that observed for MMOH-**Q**, it has been proposed that at least one other bridge is present that further constrains the metal – metal separation. This third bridge has been suggested to be a carboxylate, which is a recurring feature (E144) in all the active site structures of MMOH reported thus far.[3h, 104] Although no carboxylate-bridged $M_2(\mu\text{-}O)_2$ complex has thus far been characterized, structural studies of synthetic bis(μ-hydroxo)diiron(III,III) complexes have shown that the Fe – Fe distance progressively shrinks from 3.11 to 2.88 Å with the addition of carboxylate bridges (Table 3, entries 14 – 16).[56, 57, 61a] The proposed $M_2(\mu\text{-}O)_2(\mu\text{-}1,3\text{-}O_2CR)_n$ ($n = 1$ or 2) core formulation also has been supported by DFT calculations.[105]

Our understanding of the nature of high-valent intermediate **X** of the diiron ribonucleotide reductase, the species responsible for the formation of the catalytically essential tyrosyl radical, has also been enhanced by the synthesis and characterization of the Fe_2O_2 complexes. This intermediate was described initially as a diiron(III,III) unit coupled to a ligand radical,[106] but was better formulated later as an iron(III)iron(IV) complex.[107] This reformulation coincided with the availability of the iron(III)iron(IV) complex $[(6\text{-Metpa})_2Fe_2(O)_2]^{3+}$,[50] which exhibited similar EPR and Mössbauer properties and supported the reinterpretation of the spectroscopic data. EXAFS analysis of the iron(III)iron(IV) core of intermediate **X** revealed an Fe – Fe distance as short as that for MMOH-**Q**,[108] consistent with the presence of an $Fe_2(\mu\text{-}O)_2$ core. However, ^{17}O electron nuclear double resonance (ENDOR) studies indicated a different structure comprising only one oxo bridge and a terminal hydroxide,[109] which may derive from a ring-opening core isomerization similar to that established for $[(6\text{-}Me_3tpa)_2Fe_2(O)_2]^{3+}$.[53] To rationalize the short Fe – Fe distance, it is thought that an additional single-atom bridge from another ligand is present. The most plausible formulation consistent with the accumulated data is an $[Fe_2(\mu\text{-}O)(\mu\text{-}1,1\text{-}O_2CR)(\mu\text{-}1,3\text{-}O_2CR)]^{3+}$ core.

Lastly, $Mn_2(\mu\text{-}O)_2$ cores are almost certainly components of the tetramanganese cluster involved in the conversion of water into O_2 in the oxygen-evolving complex of photosystem II, as indicated by the presence of Mn–Mn distances of 2.7 Å in the various EXAFS analyses of this system.[66] The fact that a $M_2(\mu\text{-}\eta^2\text{:}\eta^2\text{-}O_2)/M_2(\mu\text{-}O)_2$ core isomerization can occur in copper chemistry has led to the speculation that such a process may serve as the initial step towards oxygen evolution. Although quite attractive, this intriguing mechanism remains to be demonstrated for synthetic manganese complexes and for the biological entity.

In summary, we have surveyed the range of iron and copper chemistry that provides access to novel high-valent complexes with $M_2(\mu\text{-}O)_2$ cores. Although they have different electronic structures, the cores are generally structurally analogous and have in common a high degree of covalency in their metal–oxo bonding. In addition, the cores have remarkably similar Raman and EXAFS signatures, which have served as useful spectroscopic probes. They also exhibit analogous reactivity, particularly with respect to their capability to abstract hydrogen atoms from substrates. Some copper complexes have the thus far unique property of undergoing a rapid core isomerization that reversibly forms an O–O bond between the oxo bridges, while for iron a bridge-to-terminal oxo migration process has been identified. These core isomerizations illustrate how flat the oxygen activation reactivity landscape can be. The synthesis of complexes with $Fe_2(\mu\text{-}O)_2$ and $Cu_2(\mu\text{-}O)_2$ cores has opened up a new chapter in bioinorganic enzymology; it is an effort that demonstrates the important role biomimetic studies can play in advancing our understanding of metalloenzyme systems.

8. Addendum

Since submission of this manuscript, several publications have appeared that describe relevant work. Full descriptions of the properties and reactivity of several bis(μ-oxo)dicobalt-(III,III) and -dinickel(III,III) complexes with tridentate N3 ligands have been reported.[110, 111] Intermolecular oxo transfer to sulfides from a bis(μ-oxo)dicopper(III,III) unit has been discovered,[112] but the role of this core in aromatic hydroxylation by tyrosinase was questioned in a theoretical study.[113] A new example of a neutral $Cu_2(\mu\text{-}O)_2$ complex was reported with the use of sterically hindered β-diketiminate ligands.[114] Finally, a novel bis(μ-oxo)diiron(IV,IV) complex relevant to MMO intermediate **Q** was isolated and identified on the basis of Mössbauer, resonance Raman, and EXAFS data.[115]

We are indebted to the students and postdoctoral associates who have contributed to the research in our laboratories and whose names are listed in the references. In addition, we thank the NIH (GM38767 to L.Q., GM47365 to W.B.T.) and the NSF (MCB9808350 to L.Q.) for financial support. Special thanks are due to Dr. John Hagadorn for his initial work on this review and M. Henson and E. I. Solomon for providing Figure 8.

Received: July 16, 2001 [A485]

[1] Distinguishing between these two possibilities is a challenging task, as discussed in: K. U. Ingold, P. A. MacFaul in *Biomimetic Oxidations Catalyzed by Transition Metal Complexes* (Ed.: B. Meunier), Imperial College Press, London, **2000**, p. 45.

[2] Selected reviews: a) P. R. Ortiz de Montellano, *Cytochrome P-450: Structure, Mechanism, and Biochemistry*, 2nd ed., Plenum, New York, **1995**; b) J. L. McLain, J. Lee, J. T. Groves in ref. [1] p. 91; c) B. Meunier, J. Bernadou *Structure and Bonding (Berlin)* **2000**, *97*, 1; d) D. L. Wertz, J. S. Valentine *Structure and Bonding (Berlin)* **2000**, *97*, 37; e) Y. Watanabe, H. Fujii *Structure and Bonding (Berlin)* **2000**, *97*, 61; f) M. Sono, M. P. Roach, J. H. Dawson, *Chem. Rev.* **1996**, *96*, 2841; g) B. Meunier, *Chem. Rev.* **1992**, *92*, 1411; h) M. Momenteau, C. A. Reed, *Chem. Rev.* **1994**, *94*, 659.

[3] a) B. J. Wallar, J. D. Lipscomb, *Chem. Rev.* **1996**, *96*, 2625; b) A. L. Feig, S. J. Lippard, *Chem. Rev.* **1994**, *94*, 759; c) J. Stubbe, W. A. van der Donk, *Chem. Rev.* **1998**, *98*, 705; d) E. I. Solomon, U. M. Sundaram, T. E. Machonkin, *Chem. Rev.* **1996**, *96*, 2563; e) E. I. Solomon, T. C. Brunold, M. I. Davis, J. N. Kemsley, S.-K. Lee, N. Lehnert, F. Neese, A. J. Skulan, Y.-S. Yang, J. Zhou, *Chem. Rev.* **2000**, *100*, 235; f) A. Sánchez-Ferrer, J. N. Rodríguez-López, F. García-Cánovas, F. García-Carmona, *Biochim. Biophys. Acta* **1995**, *1247*, 1; g) T. Klabunde, C. Eicken, J. C. Sacchettini, B. Krebs, *Nat. Struct. Biol.* **1998**, *5*, 1084; h) M. Merkx, D. A. Kopp, M. H. Sazinsky, J. L. Blazyk, J. Müller, S. J. Lippard, *Angew. Chem.* **2001**, *113*, 2860; *Angew. Chem. Int. Ed.* **2001**, *40*, 2782; i) E. I. Solomon, P. Chen, M. Metz, S.-K. Lee, A. E. Palmer, *Angew. Chem.* **2001**, *113*, 4702; *Angew. Chem. Int. Ed.* **2001**, *40*, 4570.

[4] a) J. A. Broadwater, J. Ai, T. M. Loehr, J. Sanders-Loehr, B. G. Fox, *Biochemistry* **1998**, *37*, 14664; b) P. Moënne-Loccoz, J. Baldwin, B. A. Ley, T. M. Loehr, J. J. M. Bollinger, *Biochemistry* **1998**, *37*, 14659; c) P. Moënne-Loccoz, C. Krebs, K. Herlihy, D. E. Edmondson, E. C. Theil, B. H. Huynh, T. M. Loehr, *Biochemistry* **1999**, *38*, 5290; d) J. Hwang, C. Krebs, B. H. Huynh, D. E. Edmondson, E. C. Theil, J. E. Penner-Hahn, *Science* **2000**, *287*, 122.

[5] K. D. Karlin, *Science* **1993**, *261*, 701.

[6] a) M. Fontecave, S. Ménage, C. Duboc-Toia, *Coord. Chem. Rev.* **1998**, *178–180*, 1555; b) J. D. Bois, T. J. Mizoguchi, S. J. Lippard, *Coord. Chem. Rev.* **2000**, *200–202*, 443; c) J.-J. Girerd, F. Banse, A. J. Simaan, *Struct. Bonding (Berlin)* **2000**, *97*, 145; d) M. Costas, K. Chen, L. Que, Jr., *Coord. Chem. Rev.* **2000**, *200–202*, 517.

[7] Y. N. Belokon, S. C. Cepas, B. Green, N. S. Ikonnikov, V. N. Khrustalev, V. S. Larichev, M. A. Moscalenk, M. North, C. Orizu, V. I. Tararov, M. Tararov, M. Tasinazzo, G. I. Timofeeva, L. V. Yashkina, *J. Am. Chem. Soc.* **1999**, *121*, 3968, and references therein.

[8] Z. Duan, M. Schmidt, V. G. Young, Jr., X. Xie, R. E. McCarley, J. G. Verkade, *J. Am. Chem. Soc.* **1996**, *118*, 5302.

[9] H. Nishino, J. K. Kochi, *Inorg. Chim. Acta* **1990**, *174*, 93.

[10] a) R. Manchanda, G. W. Brudvig, R. H. Crabtree, *Coord. Chem. Rev.* **1995**, *144*, 1; b) K. Wieghardt, *Angew. Chem.* **1989**, *101*, 1179; *Angew. Chem. Int. Ed. Engl.* **1989**, *28*, 1153.

[11] a) W. B. Tolman, *Acc. Chem. Res.* **1997**, *30*, 227; b) P. L. Holland, W. B. Tolman, *Coord. Chem. Rev.* **1999**, *190–192*, 855.

[12] a) L. Que, Jr., Y. Dong, *Acc. Chem. Res.* **1996**, *29*, 190; b) L. Que, Jr., *J. Chem. Soc. Dalton Trans.* **1997**, 3933.

[13] V. Mahadevan, R. J. M. Klein-Gebbink, T. D. P. Stack, *Curr. Opin. Chem. Biol.* **2000**, *4*, 228.

[14] S. Hikichi, M. Yoshizawa, Y. Sasakura, M. Akita, Y. Moro-Oka, *J. Am. Chem. Soc.* **1998**, *120*, 10567.

[15] K. Shiren, S. Ogo, S. Fujinami, H. Hayashi, M. Suzuki, A. Uehara, Y. Watanabe, Y. Moro-oka, *J. Am. Chem. Soc.* **2000**, *122*, 254.

[16] S. Itoh, H. Bandoh, S. Nagatomo, T. Kitagawa, S. Fukuzumi, *J. Am. Chem. Soc.* **1999**, *121*, 8945.

[17] B. S. Mandimutsira, J. L. Yamarik, T. C. Brunold, W. Gu, S. P. Cramer, C. G. Riordan, *J. Am. Chem. Soc.* **2001**, *123*, 9194.

[18] a) K. D. Karlin, A. D. Zuberbühler in *Bioinorganic Catalysis*, 2nd ed (Ed.: J. Reedijk), Marcel Dekker, New York, **1999**, p. 469; b) M.-A. Kopf, K. D. Karlin in ref. [1], p. 309; c) A. G. Blackman, W. B. Tolman in *Structure and* Bonding *(Berlin)* **2000**, *97*, 179; d) N. Kitajima, Y. Moro-oka, *Chem. Rev.* **1994**, *94*, 737.

[19] J. Kim, Y. Dong, E. Larka, L. Que, Jr., *Inorg. Chem.* **1996**, *35*, 2369.

[20] S. Mahapatra, J. A. Halfen, E. C. Wilkinson, G. Pan, C. J. Cramer, L. Que, Jr., W. B. Tolman, *J. Am. Chem. Soc.* **1995**, *117*, 8865.

[21] J. A. Halfen, S. Mahapatra, E. C. Wilkinson, S. Kaderli, V. G. Young, Jr., L. Que, Jr., A. D. Zuberbühler, W. B. Tolman, *Science* **1996**, *271*, 1397.

[22] S. Mahapatra, J. A. Halfen, E. C. Wilkinson, G. Pan, X. Wang, V. G. Young, Jr., C. J. Cramer, L. Que, Jr., W. B. Tolman, *J. Am. Chem. Soc.* **1996**, *118*, 11555.

[23] S. Mahapatra, V. G. Young, Jr., W. B. Tolman, *Angew. Chem.* **1997**, *109*, 125; *Angew. Chem. Int. Ed. Engl.* **1997**, *36*, 130.

[24] S. Mahapatra, S. Kaderli, A. Llobet, Y.-M. Neuhold, T. Palanché, J. A. Halfen, V. G. Young, Jr., T. A. Kaden, L. Que, Jr., A. D. Zuberbühler, W. B. Tolman, *Inorg. Chem.* **1997**, *36*, 6343.

[25] P. L. Holland, K. R. Rodgers, W. B. Tolman, *Angew. Chem.* **1999**, *111*, 1210; *Angew. Chem. Int. Ed.* **1999**, *38*, 1139.

[26] V. Mahadevan, Z. Hou, A. P. Cole, D. E. Root, T. K. Lal, E. I. Solomon, T. D. P. Stack, *J. Am. Chem. Soc.* **1997**, *119*, 11996.
[27] S. Itoh, M. Taki, H. Nakao, P. L. Holland, W. B. Tolman, L. Que, Jr., S. Fukuzumi, *Angew. Chem.* **2000**, *112*, 409; *Angew. Chem. Int. Ed.* **2000**, *39*, 398.
[28] E. Pidcock, S. DeBeer, H. V. Obias, B. Hedman, K. O. Hodgson, K. D. Karlin, E. I. Solomon, *J. Am. Chem. Soc.* **1999**, *121*, 1870.
[29] B. M. T. Lam, J. A. Halfen, V. G. Young, Jr., J. R. Hagadorn, P. L. Holland, A. Lledós, L. Cucurull-Sánchez, J. J. Novoa, S. Alvarez, W. B. Tolman, *Inorg. Chem.* **2000**, *39*, 4059.
[30] H. Hayashi, S. Fujinami, S. Nagatomo, S. Ogo, M. Suzuki, A. Uehara, Y. Watanabe, T. Kitagawa, *J. Am. Chem. Soc.* **2000**, *122*, 2124.
[31] M. Enomoto, T. Aida, *J. Am. Chem. Soc.* **1999**, *121*, 874.
[32] B. F. Straub, F. Rominger, P. Hofmann, *Chem. Commun.* **2000**, 1611.
[33] V. Mahadevan, M. J. Henson, E. I. Solomon, T. D. P. Stack, *J. Am. Chem. Soc.* **2000**, *122*, 10249.
[34] V. Mahadevan, J. L. DuBois, B. Hedman, K. O. Hodgson, T. D. P. Stack, *J. Am. Chem. Soc.* **1999**, *121*, 5583.
[35] H. V. Obias, Y. Lin, N. N. Murthy, E. Pidcock, E. I. Solomon, M. Ralle, N. J. Blackburn, Y. M. Neubold, A. D. Zuberbühler, K. D. Karlin, *J. Am. Chem. Soc.* **1998**, *120*, 12960.
[36] M. Taki, S. Itoh, S. Fukuzumi, *J. Am. Chem. Soc.* **2001**, *123*, 6203.
[37] Y. Funahashi, K. Nakaya, S. Hirota, O. Yamauchi, *Chem. Lett.* **2000**, 1172.
[38] a) N. Wei, N. N. Murthy, Q. Chen, J. Zubieta, K. D. Karlin, *Inorg. Chem.* **1994**, *33*, 1953; b) K. Fujisawa, M. Tanaka, Y. Moro-oka, N. Kitajima, *J. Am. Chem. Soc.* **1994**, *116*, 12079.
[39] J. Cahoy, P. L. Holland, W. B. Tolman, *Inorg. Chem.* **1999**, *38*, 2161.
[40] S. Itoh, H. Nakao, L. M. Berreau, T. Kondo, M. Komatsu, S. Fukuzumi, *J. Am. Chem. Soc.* **1998**, *120*, 2890.
[41] K. D. Karlin, W. B. Tolman, S. Kaderli, A. D. Zuberbühler, *J. Mol. Catal. A* **1997**, *117*, 215.
[42] Y. Zang, Y. Dong, L. Que, Jr., K. Kauffmann, E. Münck, *J. Am. Chem. Soc.* **1995**, *117*, 1169.
[43] H. Zheng, Y. Zang, Y. Dong, V. G. Young, Jr., L. Que, Jr., *J. Am. Chem. Soc.* **1999**, *121*, 2226.
[44] E. J. Larson, P. J. Riggs, J. E. Penner-Hahn, V. L. Pecoraro, *J. Chem. Soc. Chem. Commun.* **1992**, 102.
[45] B. G. Gafford, R. A. Holwerda, *Inorg. Chem.* **1989**, *28*, 60.
[46] Y. Zang, G. Pan, L. Que, Jr., B. G. Fox, E. Münck, *J. Am. Chem. Soc.* **1994**, *116*, 3653.
[47] H. Furutachi, Y. Ohyama, Y. Tsuchiya, K. Hashimoto, S. Fujinami, A. Uehara, M. Suzuki, Y. Maeda, *Chem. Lett.* **2000**, 1132.
[48] a) R. A. Leising, B. A. Brennan, L. Que, Jr., B. G. Fox, E. Münck, *J. Am. Chem. Soc.* **1991**, *113*, 3988; b) Y. Dong, H. Fujii, M. P. Hendrich, R. A. Leising, G. Pan, C. R. Randall, E. C. Wilkinson, Y. Zang, L. Que, Jr., B. G. Fox, K. Kauffmann, E. Münck, *J. Am. Chem. Soc.* **1995**, *117*, 2778.
[49] H.-F. Hsu, Y. Dong, L. Shu, V. G. Young, Jr., L. Que, Jr., *J. Am. Chem. Soc.* **1999**, *121*, 5230.
[50] Y. Dong, L. Que, Jr., K. Kauffmann, E. Münck, *J. Am. Chem. Soc.* **1995**, *117*, 11377.
[51] Y. Dong, Y. Zang, L. Shu, E. C. Wilkinson, L. Que, Jr., K. Kauffmann, E. Münck, *J. Am. Chem. Soc.* **1997**, *119*, 12683.
[52] V. L. MacMurdo, H. Zheng, L. Que, Jr., *Inorg. Chem.* **2000**, *39*, 2254.
[53] H. Zheng, S. J. Yoo, E. Münck, L. Que, Jr., *J. Am. Chem. Soc.* **2000**, *122*, 3789.
[54] D. Lee, J. D. Bois, D. Petasis, M. P. Hendrich, C. Krebs, B. H. Huynh, S. J. Lippard, *J. Am. Chem. Soc.* **1999**, *121*, 9893.
[55] A delocalized mixed-valent $S=\frac{1}{2}$ diiron(II,II) compound was prepared by chemical oxidation of a diiron(II,II) precursor, and on the basis of spectroscopic analogies it is presumably the same species as that present in the green solution derived from the oxygenation reaction: D. Lee, C. Krebs, B. H. Huynh, M. P. Hendrich, S. J. Lippard, *J. Am. Chem. Soc.* **2000**, *122*, 5000.
[56] D. Lee, S. J. Lippard, *J. Am. Chem. Soc.* **2001**, *123*, 4611.
[57] D. Lee, S. J. Lippard, *J. Am. Chem. Soc.* **1998**, *120*, 12153.
[58] N. Kitajima, K. Fujisawa, C. Fujimoto, Y. Moro-oka, S. Hashimoto, T. Kitagawa, K. Toriumi, K. Tatsumi, A. Nakamura, *J. Am. Chem. Soc.* **1992**, *114*, 1277.
[59] A (peroxo)dicopper(II,II) complex with a short Cu···Cu distance of 2.84 Å as determined by EXAFS analysis has been reported: C. He, J. L. DuBois, B. Hedman, K. O. Hodgson, S. J. Lippard, *Angew. Chem.* **2001**, *113*, 1532; *Angew. Chem. Int. Ed.* **2001**, *40*, 1484.
[60] K. A. Magnus, B. Hazes, H. Ton-That, C. Bonaventura, J. Bonaventura, W. G. J. Hol, *Proteins* **1994**, *19*, 302.
[61] a) J. A. Thich, C. C. Ou, D. Powers, B. Vasiliou, D. Mastropaolo, J. A. Potenza, J. H. Schugar, *J. Am. Chem. Soc.* **1976**, *98*, 1425; b) C. C. Ou, R. A. Lalancette, J. A. Potenza, H. Schugar, *J. Am. Chem. Soc.* **1978**, *100*, 2053; c) L. Borer, L. Thalken, C. Ceccarelli, M. Glick, J. H. Zhang, W. M. Reiff, *Inorg. Chem.* **1983**, *22*, 1719; d) S. Ménage, L. Que, Jr., *Inorg. Chem.* **1990**, *29*, 4293; e) J. A. Bertrand, P. G. Eller, *Inorg. Chem.* **1974**, *13*, 927; f) B. Chiari, O. Piovesana, T. Tarantelli, P. F. Zanazzi, *Inorg. Chem.* **1982**, *21*, 2444; g) B. Chiari, O. Piovesana, T. Tarantelli, P. F. Zanazzi, *Inorg. Chem.* **1984**, *23*, 3398.
[62] D. M. Kurtz, Jr., *Chem. Rev.* **1990**, *90*, 585.
[63] a) M. J. Baldwin, T. L. Stemmler, P. J. Riggs-Gelasco, M. L. Kirk, J. E. Penner-Hahn, V. L. Pecoraro, *J. Am. Chem. Soc.* **1994**, *116*, 11349; b) M. J. Baldwin, V. Pecoraro, *J. Am. Chem. Soc.* **1996**, *118*, 11325.
[64] N. J. Hardman, P. P. Power, *J. Am. Chem. Soc.* **2001**, *123*, 2474.
[65] R. A. Scott in *Physical Methods in Bioinorganic Chemistry: Spectroscopy and Magnetism* (Ed.: L. Que, Jr.), University Science Books, Sausalito, CA, **2000**, p. 465.
[66] V. K. Yachandra, K. Sauer, M. P. Klein, *Chem. Rev.* **1996**, *96*, 2927.
[67] E. C. Wilkinson, Y. Dong, Y. Zang, H. Fujii, R. Fraczkiewicz, G. Fraczkiewicz, R. S. Czernuszewicz, L. Que, Jr., *J. Am. Chem. Soc.* **1998**, *120*, 955.
[68] M. J. Henson, P. Mukherjee, D. E. Root, T. D. P. Stack, E. I. Solomon, *J. Am. Chem. Soc.* **1999**, *121*, 10332.
[69] P. L. Holland, C. J. Cramer, E. C. Wilkinson, S. Mahapatra, K. R. Rodgers, S. Itoh, M. Taki, S. Fukuzumi, L. Que, Jr., W. B. Tolman, *J. Am. Chem. Soc.* **2000**, *122*, 792.
[70] J. Sanders-Loehr, W. D. Wheeler, A. K. Shiemke, B. A. Averill, T. M. Loehr, *J. Am. Chem. Soc.* **1989**, *111*, 8084.
[71] C. E. MacBeth, A. P. Golumbek, V. G. Young, Jr., C. Yang, K. Kuczera, M. P. Hendrich, A. S. Borovik, *Science* **2000**, *289*, 938.
[72] R. E. Norman, S. Yan, L. Que, Jr., J. Sanders-Loehr, G. Backes, J. Ling, J. H. Zhang, C. J. O'Connor, *J. Am. Chem. Soc.* **1990**, *112*, 1554.
[73] N5 = *N*-(hydroxyethyl)-*N*,*N*′,*N*′-tris(2-benzimidazolylmethyl)-1,2-diaminoethane. P. Gómez-Romero, E. H. Witten, W. M. Reiff, G. Backes, J. Sanders-Loehr, G. B. Jameson, *J. Am. Chem. Soc.* **1989**, *111*, 9039.
[74] J. D. Cohen, S. Payne, K. S. Hagen, J. Sanders-Loehr, *J. Am. Chem. Soc.* **1997**, *119*, 2960.
[75] A. Nanthakumar, M. S. Nasir, K. D. Karlin, N. Ravi, B. H. Huynh, *J. Am. Chem. Soc.* **1992**, *114*, 6564.
[76] a) I. D. Brown, D. Altermatt, *Acta Crystallogr. Sect. B* **1985**, *41*, 244; b) H. H. Thorp, *Inorg. Chem.* **1992**, *31*, 1585; c) S. Hati, D. Datta, *J. Chem. Soc. Dalton Trans.* **1995**, 1177; d) S. M. Kanowitz, G. J. Palenik, *Inorg. Chem.* **1998**, *37*, 2086; e) H. H. Thorp, *Inorg. Chem.* **1998**, *37*, 5690.
[77] a) J. L. DuBois, P. Mukherjee, A. M. Collier, J. M. Mayer, E. I. Solomon, B. Hedman, T. D. P. Stack, K. O. Hodgson, *J. Am. Chem. Soc.* **1997**, *119*, 8578; b) J. L. DuBois, P. Mukherjee, T. D. P. Stack, B. Hedman, E. I. Solomon, K. O. Hodgson, *J. Am. Chem. Soc.* **2000**, *122*, 5775.
[78] C. J. Cramer, B. A. Smith, W. B. Tolman, *J. Am. Chem. Soc.* **1996**, *118*, 11283.
[79] a) X.-Y. Liu, A. A. Palacios, J. J. Novoa, S. Alvarez, *Inorg. Chem.* **1998**, *37*, 1202; b) M. Flock, K. Pierloot, *J. Phys. Chem. A* **1999**, *103*, 95; c) R. Lind, P. E. M. Siegbahn, R. H. Crabtree, *J. Phys. Chem. B* **1999**, *103*, 1193.
[80] E. I. Solomon, F. Tuczek, D. E. Root, C. A. Brown, *Chem. Rev.* **1994**, *94*, 827.
[81] C. A. Brown, G. J. Remar, R. L. Musselman, E. I. Solomon, *Inorg. Chem.* **1995**, *34*, 688.
[82] R. E. Norman, R. C. Holz, S. Ménage, C. J. O'Connor, J. H. Zhang, L. Que, Jr., *Inorg. Chem.* **1990**, *29*, 4629.
[83] S. M. Gorun, S. J. Lippard, *Inorg. Chem.* **1991**, *30*, 1625.
[84] a) B. E. Sturgeon, D. Burdi, S. Chen, B.-H. Huynh, D. E. Edmondson, J. Stubbe, B. M. Hoffman, *J. Am. Chem. Soc.* **1996**, *118*, 7551; b) A. M. Valentine, P. Tavares, A. S. Pereira, R. Davydov, C. Krebs,

B. M. Hoffman, D. E. Edmonson, B. H. Huynh, S. J. Lippard, *J. Am. Chem. Soc.* **1998**, *120*, 2190.
[85] A. Ghosh, J. Almlöf, L. Que, Jr., *Angew. Chem.* **1996**, *108*, 846; *Angew. Chem. Int. Ed. Engl.* **1996**, *35*, 770.
[86] D. M. Proserpio, R. Hoffmann, G. C. Dismukes, *J. Am. Chem. Soc.* **1992**, *114*, 4374.
[87] a) P. E. M. Siegbahn, *J. Biol. Inorg. Chem.* **2001**, *6*, 27; b) K. Yoshizawa, T. Ohta, T. Yamabe, R. Hoffmann, *J. Am. Chem. Soc.* **1997**, *119*, 12311.
[88] a) T. Ookubo, H. Sugimoto, T. Nagayama, H. Masuda, T. Sata, K. Tanaka, Y. Maeda, H. Okawa, Y. Hayashi, A. Uehara, M. Suzuki, *J. Am. Chem. Soc.* **1996**, *118*, 701; b) Y. Dong, S. Yan, V. G. Young, Jr., L. Que, Jr., *Angew. Chem.* **1996**, *108*, 674; *Angew. Chem. Int. Ed. Engl.* **1996**, *35*, 618; c) K. Kim, S. J. Lippard, *J. Am. Chem. Soc.* **1996**, *118*, 4914.
[89] H.-F. Hsu, H. Zheng, L. Que, Jr., unpublished observations.
[90] S. Mahapatra, J. A. Halfen, W. B. Tolman, *J. Am. Chem. Soc.* **1996**, *118*, 11575.
[91] A. Kohen, J. P. Klinman, *Acc. Chem. Res.* **1998**, *31*, 397.
[92] J. C. Nesheim, J. D. Lipscomb, *Biochemistry* **1996**, *35*, 10240.
[93] This value $\rho = -0.4$ differs from and should be used instead of that originally published in ref. [90] ($\rho = -0.8$). The latter value is in error because it was derived from the slope of the line fit to a plot of $\ln(k)$ versus σ^+; analysis of a plot of $\log(k)$ versus σ^+ (using the correct, published rate constants) yields the correct value. Use of the correct ρ value does not necessitate any change in the discussion or conclusions drawn in ref. [90].
[94] a) G. A. Russell in *Free Radicals*, *Vol. I* (Ed.: J. K. Kochi), Wiley, New York, **1973**, p. 275; b) A. D. N. Vaz, M. J. Coon, *Biochemistry* **1994**, *33*, 6442; c) P. Inchley, J. R. L. Smith, R. J. Lower, *New J. Chem.* **1989**, *13*, 669.
[95] a) M. Newcomb, P. H. Toy, *Acc. Chem. Res.* **2000**, *33*, 449; b) A. M. Valentine, M. LeTadic-Biadatti, P. H. Toy, M. Newcomb, S. J. Lippard, *J. Biol. Chem.* **1999**, *274*, 10771; c) F. Ogliaro, N. Harris, S. Cohen, M. Filatov, S. P. de Visser, S. Shaik, *J. Am. Chem. Soc.* **2000**, *122*, 8977.
[96] C. J. Cramer, Y. Pak, *Theor. Chem. Acc.* **2000**, *105*, 477.
[97] a) I. Blain, P. Bruno, M. Giorgi, E. Lojou, D. Lexa, M. Réglier, *Eur. J. Inorg. Chem.* **1998**, 1297; b) I. Blain, M. Giorgi, I. D. Riggi, M. Réglier, *Eur. J. Inorg. Chem.* **2000**, 393; c) I. Blain, M. Giorgi, I. D. Riggi, M. Réglier, *Eur. J. Inorg. Chem.* **2001**, 205.
[98] L. M. Berreau, S. Mahapatra, J. A. Halfen, R. P. Houser, V. G. Young, Jr., W. B. Tolman, *Angew. Chem.* **1999**, *111*, 180; *Angew. Chem. Int. Ed.* **1999**, *38*, 207.
[99] C. Eicken, F. Zippel, K. Büldt-Karentzopoulos, B. Krebs, *FEBS Lett.* **1998**, *436*, 293.
[100] S. Itoh, H. Kumei, M. Taki, S. Nagatomo, T. Kitagawa, S. Fukuzumi, *J. Am. Chem. Soc.* **2001**, *123*, 6708.
[101] E. Pidcock, H. V. Obias, C. X. Zhang, K. D. Karlin, E. I. Solomon, *J. Am. Chem. Soc.* **1998**, *120*, 7841.
[102] C. Kim, Y. Dong, L. Que, Jr., *J. Am. Chem. Soc.* **1997**, *119*, 3635.
[103] H. Decker, R. Dillinger, F. Tuczek, *Angew. Chem.* **2000**, *112*, 1656; *Angew. Chem. Int. Ed.* **2000**, *39*, 1591.
[104] a) A. C. Rosenzweig, C. A. Frederick, S. J. Lippard, P. Nordlund, *Nature* **1993**, *366*, 537; b) A. C. Rosenzweig, P. Nordlund, P. M. Takahara, C. A. Frederick, S. J. Lippard, *Chem. Biol.* **1995**, *2*, 409; c) N. Elango, R. Radhakrishnan, W. A. Froland, B. J. Wallar, C. A. Earhart, J. D. Lipscomb, D. H. Ohlendorf, *Protein Sci.* **1997**, *6*, 556; d) A. C. Rosenzweig, H. Brandstetter, D. A. Whittington, P. Nordlund, S. J. Lippard, C. A. Frederick, *Proteins Struct. Funct. Genet.* **1997**, *29*, 141; e) D. A. Whittington, S. J. Lippard, *J. Am. Chem. Soc.* **2001**, *123*, 827; f) D. A. Whittington, M. H. Sazinsky, S. J. Lippard, *J. Am. Chem. Soc.* **2001**, *123*, 1794.
[105] a) B. F. Gherman, B. D. Dunietz, D. A. Whittington, S. J. Lippard, R. A. Friesner, *J. Am. Chem. Soc.* **2001**, *123*, 3836; b) B. D. Dunietz, M. D. Beachy, Y. Cao, D. A. Whittington, S. J. Lippard, R. A. Friesner, *J. Am. Chem. Soc.* **2000**, *122*, 2828; c) P. E. M. Siegbahn, *Inorg. Chem.* **1999**, *38*, 2880; d) H. Basch, K. Mogi, D. G. Musaev, K. Morokuma, *J. Am. Chem. Soc.* **1999**, *121*, 7249.
[106] N. Ravi, J. M. Bollinger, Jr., B. H. Huynh, D. E. Edmondson, J. Stubbe, *J. Am. Chem. Soc.* **1994**, *116*, 8007.
[107] B. E. Sturgeon, D. Burdi, S. Chen, B.-H. Huynh, D. E. Edmondson, J. Stubbe, B. M. Hoffman, *J. Am. Chem. Soc.* **1996**, *118*, 7551.
[108] P. J. Riggs-Gelasco, L. Shu, S. Chen, D. Burdi, B. H. Huynh, L. Que, Jr., J. Stubbe, *J. Am. Chem. Soc.* **1998**, *120*, 849.
[109] D. Burdi, J. P. Willems, P. J. Riggs-Gelasco, W. E. Antholine, J. Stubbe, B. M. Hoffman, *J. Am. Chem. Soc.* **1998**, *120*, 12910.
[110] S. Itoh, H. Bandoh, M. Nakagawa, S. Nagatomo, T. Kitagawa, K. D. Karlin, S. Fukuzumi, *J. Am. Chem. Soc.* **2001**, *123*, 11168.
[111] S. Hikichi, M. Yoshizawa, Y. Sasakura, H. Komatsuzaki, Y. Morooka, M. Akita, *Chem. Eur. J.* **2001**, *7*, 5012.
[112] M. Taki, S. Itoh, S. Fukuzumi, *J. Am. Chem. Soc.* **2002**, *124*, 998.
[113] P. E. M. Siegbahn, M. Wirstam, *J. Am. Chem. Soc.* **2001**, *123*, 11819.
[114] D. J. E. Spencer, N. W. Aboelella, A. M. Reynolds, P. L. Holland, W. B. Tolman, *J. Am. Chem. Soc.* **2002**, *124*, in press.
[115] M. Costas, J.-U. Rohde, A. Stubna, R. Y. N. Ho, L. Quaroni, E. Münck, L. Que, Jr., *J. Am. Chem. Soc.* **2001**, *123*, 12931.